CHALMERS

Analytical weight optimization of an enclosed stressed skin derrick

Master's Thesis in the International Master's Programme in Naval Architecture and Ocean Engineering

ABDULLAH BALKHI AND ALI AZIMIFAR

Department of Shipping and Marine Technology
Division of Marine Design, Research Group Marine Structures
CHALMERS UNIVERSITY OF TECHNOLOGY
Göteborg, Sweden 2013
Masters's Thesis X-13/293

Analytical weight optimization of an enclosed stressed skin derrick

ABDULLAH BALKHI AND ALI AZIMIFAR

Analytical weight optimization of an enclosed stressed skin derrick
ABDULLAH BALKHI AND ALI AZIMIFAR

Analytical weight optimization of an enclosed stressed skin derrick
Master's Thesis in the International Master's Programme in Naval Architecture and Ocean Engineering
ABDULLAH BALKHI AND ALI AZIMIFAR
Department of Shipping and Marine Technology
Division of Marine Design, Research Group Marine Structures
Chalmers University of Technology

ABSTRACT

The demand for drilling operations in Arctic regions is growing significantly due to an increasing need for oil and gas. The harsh environment in Arctic regions requires safe and acceptable working conditions. In order to still have an acceptable working environment and protection for drilling and pipe handling equipment, it is important to make improvements in design of upcoming drilling rigs. One of the items that needed to be developed is the derrick/drill tower, which today is mainly constructed as a structural framework and has limited working areas where crews can work without exposure to the weather and winds. A low structural weight of a derrick is desired in order to achieve improved and sustained stability conditions.

The objectives with the present study is to propose a weight-optimized stressed skin derrick and compare the design with a covered conventional truss derrick with respect to weight and strength.

Aker MH has provided data about a conventional truss derrick which was used as a reference derrick for input of loads, dimensions and weights in order to design a new derrick. To ensure enough structural strength against yielding and buckling, structural analyses were carried out by using a finite element analysis based on 3D beam theory. Numerical optimization of outer plating thickness, stiffeners and stringer dimensions were performed by using the numerical computation software Matlab.

After the optimization against buckling and yielding, a final weight of 465 mT was achieved. This weight can be compared to a covered conventional truss derrick which is estimated to 590 mT. The reduction of weight is 21 % compared to a covered conventional truss derrick. The vertical centre of gravity of the new derrick design was reduced by 1.5 m. By introducing radius in the corner of a stressed skin derrick, the wind forces acting on the derrick were decreased significantly and this provides sustained stability for a drilling unit. Due to lower weight in the new design, the manufacturing costs were reduced by 4.2 MNOK.

The obtained weight of the stressed skin derrick is less than the covered conventional truss derrick. In order to use the proposed design in the future, a further study should be carried out. To ensure that the designs are safe enough for commercial usage, a fatigue analysis needs to be carried out in order to achieve the final design.

Key words: Beam theory, finite element method, numerical optimization, stability, stress skin derrick, usage factor

Contents

Preface

This thesis is a part of the requirements for the master's degree in Naval Architecture at Chalmers University of Technology, Göteborg, and has been carried out at the Division of Marine Design, Department of Shipping and Marine Technology, Chalmers University of Technology. It has been written at Bassoe Technology, Gothenburg, Sweden, during the spring of 2013.

Göteborg, June, 2013

Abdullah Balkhi and Ali Azimifar

Notations and abbreviations

Symbols

α	Angle [deg]
θ	Angle [deg]
γ_F	Resistance factor [-]
γ_m	Nominal capacities [-]
η_0	Basic usage factor [-]
η_p	Usage factor [-]
ρ_a	Density of air [kg/m^3]
σ_{vM}	von Mises equivalent stresses [MPa]
$\sigma_{permissible}$	Permissible stress [MPa]
σ_x	Axial compressive stress [MPa]
σ_y	Transverse compressive stress [MPa]
$\sigma_{yielding}$	Yield stress [MPa]
τ	Shear stress [MPa]
τ_{max}	Maximum shear stress, [MPa]
τ_{xy}	Shear stress between stiffened plate [MPa]
A	Area [m^2]
B_f	Breath of flange [mm]
BM	Distance from centre of buoyancy to metacentric height [m]
C_d	Drag coefficient [-]
C_{RT}	Torsional constant [-]
E	Young's modulus [GPa]
Fw	Wind force [N]
$f(x)$	Objective function
$g_j(x)$	Inequality constraints
GM	Metacentric height [m]
GZ	Righting arm [m]
H_{10m}	Reference height [m]
$h_k(x)$	Equality constraints
I	Torsional constant [m^4]
$I_{stiffener}$	Moment of inertia of stiffener [m^4]
I_Y	Moment of inertia in the y direction [m^4]
I_Z	Moment of inertia in the z direction [m^4]
hw	Web height of stiffener and stringer [mm]
K	Spring stiffness [N/m]
KB	Distance from keel to centre of buoyancy [m]
KG	Distance from keel to centre of gravity [m]
M	Structural mass [mT]
mT	Metric ton [ton]
M_Y	Bending moment in y-direction [Nm]
M_Z	Bending moment in z-direction [Nm]
Psd	Lateral pressure [MPa]
s	Stiffener spacing [mm]
q	Basic wind pressure [N/mm^2]
R^2	Determination coefficient [%]
R/W	Radius ratio [-]
S	Projected area [m^2]

T	Averaging time period [s]
T_{60s}	Reference averaging time [s]
t, t_p	Plate thickness [mm]
t_f	Flange thickness [mm]
t_m	Thickness of primary elements [mm]
tw	Web thickness of stiffener and stringer [mm]
$U(T,z)$	Wind speed [m/s]
$U_{(10m,60s)}$	Wind speed at reference height with reference averaging time [m/s]
UF_A	Usage factor, girder web-area control [-]
UF_g	Usage factor, girder buckling check at end and mid-span [-]
UF_{lv}	Usage factor, girder shear control [-]
UF_p	Usage factor, plate buckling check [-]
UF_{plate}	Usage factor, plate lateral capacity check [-]
UF_s	Usage factor, stiffener buckling check at end and mid-span [-]
UF_t	Usage factor, minimum thickness control [-]
UF_V	Usage factor, stiffener shear capacity control [-]
UF_{yg}	Usage factor, girder yielding check [-]
UF_{yp}	Usage factor, plate yielding check [-]
UF_{vs}	Usage factor, stiffener yielding check [-]
UF_{zg}	Usage factor, minimum section modulus check for girder [-]
UF_{zp}	Usage factor, minimum section modulus check for plate [-]
UF_{zs}	Usage factor, minimum section modulus check for stiffener [-]
V	Shear force [MPa]
VCG	Vertical centre of gravity [m]
w	Displacement [m]
x	Vector with design variables
x_1	Lower boundary design variable
x_2	Upper boundary design variable
X_1	Centre of gravity of ship [m]
X_2	Centre of gravity of derrick [m]
z	Height [m]

Abbreviations

DNV	Det Norske Veritas
FE	Finite Element
FEA	Finite Element Analysis
FEM	Finite Element Method
SQP	Sequential quadratic programming
WSD	Working Stress Design
LRFD	Load and Resistance Factor Design

1 Introduction

1.1 Background and motivation of work

As the oil interest increases in the Arctic region, the demand and standards for ensuring acceptable and safe working conditions are set higher according to the Arctic Institute [1]. According to the U.S. Geological Survey report [2], the Arctic may contain one-fifth of the world's undiscovered oil and natural gas. More specifically, the Arctic region contains 90 billion barrels of undiscovered oil and 1,670 trillion cubic feet (47 trillion cubic metres of undiscovered natural gas.

Limiting working crews and equipment exposure to weather and wind is essential for workable conditions in an Arctic climate. Derricks are today mainly constructed as a structural framework and have limited areas were working crews can work without exposure. See Figure 1.1 for a typical drilling ship with a conventional truss derrick structure design by Maersk, 2011. This drilling ship operates in the Gulf of Mexico and is capable of drilling at depths of 3,500 m.

Conventional truss derrick

Figure 1.1   A typical drilling ship with a conventional truss derrick.

Today the low temperatures are the greatest engineering challenges for designing a drilling rig suitable for temperatures below -40°C. The other design problem is wind, which causes the felt temperature to be very low. Nearly the entire rig needs to be housed in order to achieve a comfortable working condition and make the drilling operation manageable.

Derricks are structurally largely affected by wave-induced motions and wind, in addition to the demanding drilling process. Consequently, they can be a notable part of the drilling ship's/semisubmersible's total weight. Additional weight is especially sensitive for semisubmersibles and limiting topside weight is crucial due to stability conditions. The derrick structure poses, together with drilling equipment, a substantial part of the topside weight and with high centre point of gravity. Therefore, an efficient derrick with a low weight is of vital interest for a drilling unit due to better stability and impacts on motion of the drilling unit. Another important benefit with a low

weight is the manufacturing cost and of being environment friendly due to lower fuel consumption and less material usage, which provide less energy consumption to produce steel from raw material.

By applying protective shell plates to an existing truss derrick, which will not contribute to the structural strength of the derrick and merely significantly increase the weight of the derrick, is not a beneficial concept for a new derrick design proposal. First, this applies to the weight of the shell plates, but also an increasing weight of the main structure of the derrick in order to sustain the higher wind and inertia loads acting on the structure. A weight estimation of the protective shell plates to cover the truss derrick and their supports were made by Aker MH [3]. This covering weight was approximately 200 mT (ton) without taking into account the reinforcement of the main structure. With covering shell plates, the total main structure weight will approximately be 590 mT with a centre of gravity of 29.5 m without the weight of the drilling and pipe handling equipment.

According to Bassoe Technology, today´s solution of derrick structure for a cold environment has protective shell plates to cover up the truss derrick, see Figure 1.2.

Bassoe Technology has come up with a solution to a fully integrated stiffened shell construction for the derrick. By using a stiffened shell construction strength can be introduced to the structure via shear. Furthermore, depending on which form the stiffened shell has, the wind load will increase on the vessel compared with a traditional framework derrick, see Section 2.1 for the influence of derrick weight on the stability of an offshore unit.

In the present study, a conventional truss derrick was chosen from Aker MH [3]. For further details about the reference derrick, see Chapter 3.
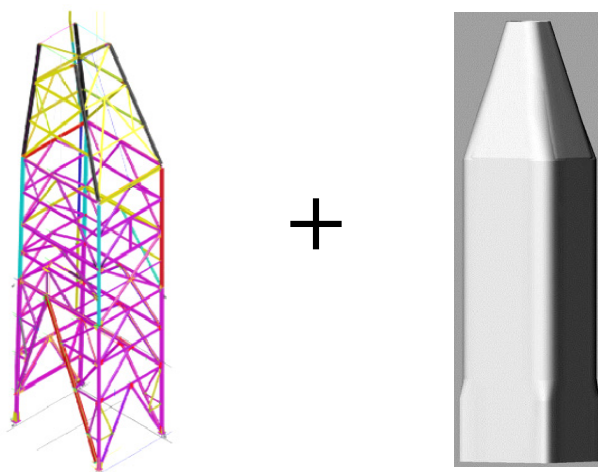
Figure 1.2   *Today´s solution of derrick structure fora cold environment. At left, a reference derrick and at right, a protective shell plate.*

1.2 Objective

The main objective of the current study was to achieve a Matlab script [4] employing a ready function in a Matlab optimization toolbox *fmincon* [5] in order to reduce the weight of the integrated shell construction for the derrick. A conventional truss derrick was chosen as a reference derrick in order to obtain the performance in aspects of strength, size, capacity, and converting it to an integrated steel panel construction instead. The goal was to create a script in Matlab to reduce the weight of the derrick shell design by altering parameters for size/shape, stiffener and stringer spacing and compare the weight to a covered conventional truss derrick. The main objective can be divided in to the following specific aims:

- Create a Matlab script which reduces the weight of the derrick shell design

- Propose an initial design of a stressed skin derrick.

- Achieve low structural weight and centre of gravity compared to the covered conventional truss derrick, namely VCG < 29.5 mT and mass < 590 mT. This will in turn also provide a sustainable design by using less raw material and energy consumption for extracting steel for the new design

- The proposed design is to be checked against buckling and yielding

- Identify the important parameters which influence both the structural strength and weight of the stressed skin derrick.

- The derrick needs to fulfil all applicable class rules, and have the sufficient space and accessibility for equipment and drilling operations.

1.3 Methodology

This chapter discusses the procedure and methodology of the present work for analysing the structure properties of the stressed skin derrick. In the current design, there was already an existing general arrangement drawing of the derrick made by Aker MH [3]. In this project, the new design of the derrick preserved the properties of the current derrick regarding the arrangement of the drilling equipment and the geometry of the interface of the derrick and the rig body. The used methods in this study aimed at restricting the redesign of structure for only influential factors for the optimization of the mass of the derrick. The study did not consider optimizing the outer geometry parameters such as length or height of the total structure.

The general procedure for the present study can be described schematically as seen in Figure 1.3. See also Section 8.3 for a more detailed methodology presentation.

The procedure in the current study was to start with arbitrary initial parameters with regard to dimensions which were bases for the calculation of mass, strength and forces acting on derrick. The stresses were obtained by using a finite element analysis based on a 3D beam theory implemented in a Matlab script [4] according to Paz and Legih [6]. The stresses were checked against buckling and yielding by using software STIPLA developed by Struprog [7] and [8] with an implemented DNV standard [9], [10] and [11]. A call script was created in Matlab to run the software STIPLA. The approved structural design of the derrick was numerically optimized against a total structural mass of the derrick. The Matlab optimization function *fmincon* was used in order to optimize the dimensions. For each dimension changes made by *fmincon*, the script of mass, strength and stresses were updated with the actual value and checked against buckling and yielding with the call script of STIPLA. The script of mass, strength, forces, stresses and STIPLA call were programmed as a run file in *fmincon* script in order to create a continued loop until the design fulfilled the design criteria with minimum structural mass.
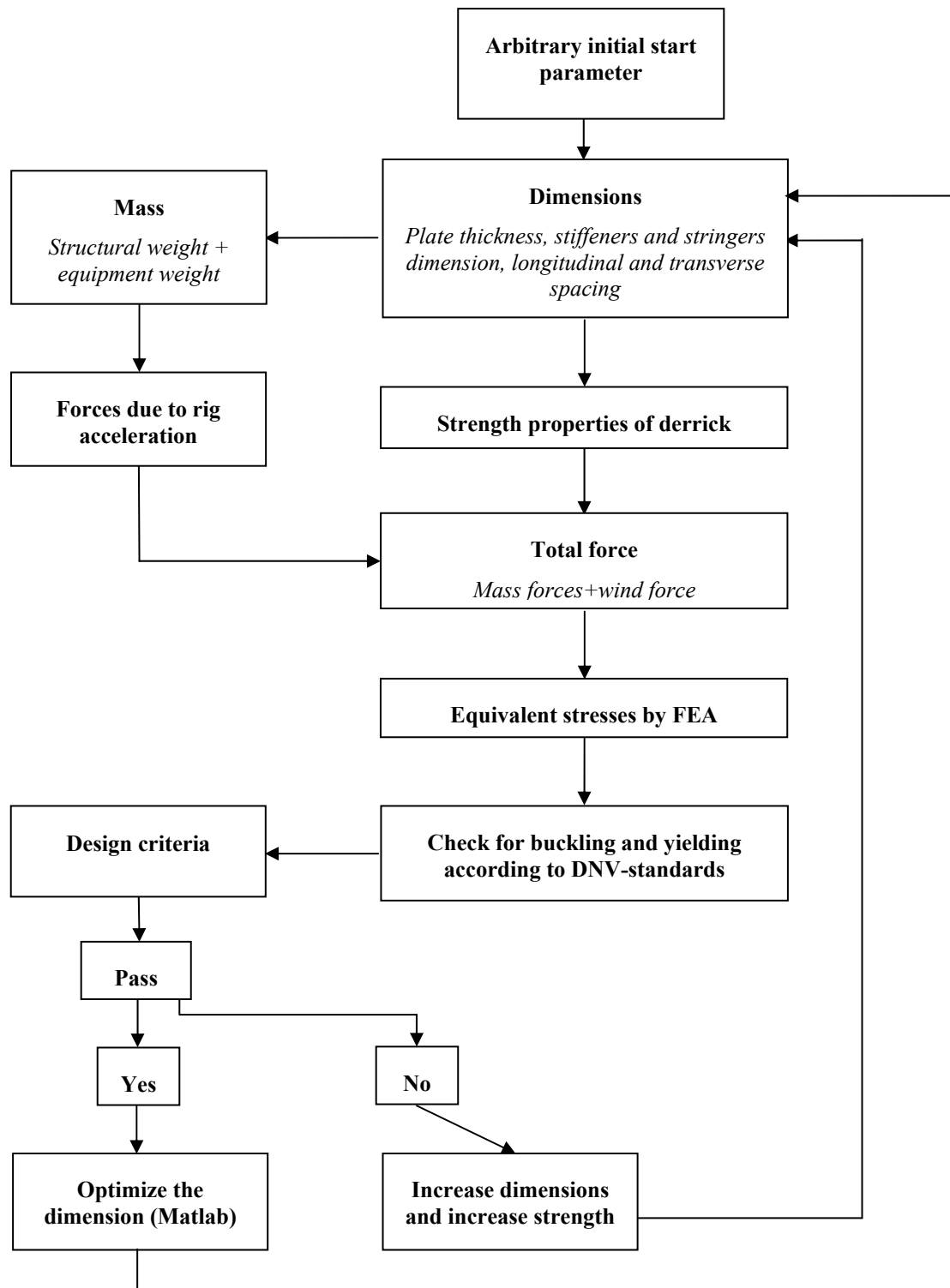
Figure 1.3   Schematic procedure of the methodology in present study.

1.4 Scope and limitation

There are several different loading conditions which have to be checked for the supported structure of a drilling unit according to DNV [9]. In the present study, only the loading condition of the derrick that gives the maximum combination of the environmental and functional load was studied. In the structural design report from Aker MH [3] for the reference derrick, operational load condition 1, which is the maximum operational load, was identified as the governing condition for the new design of derrick. In a further study all conditions must be verified.

All equipment weights in the derrick structure and the contribution of force due to rig acceleration were assumed to be constants. Due to the lack of time and available data from [3], only the location in height of the derrick was analysed for the force calculation and therefore all the equipment load assumed to be located in the centre of gravity of the derrick in the longitudinal and transverse directions. Due to this assumption, there will not be any torsional load in the derrick and torsion was not considered. For further study, the location of the equipment needs to be analysed and checked for the contribution to torsional buckling.

The proposed design of the derrick should incorporate the existing equipment with some adjustments in location due to minor changes in the design of the reference derrick. All the equipment weights in the force calculation were assumed to be constant and the same as the reference derrick in order to make the force analyses more accurate.

In the study and investigation of proposed initial design, the main dimensions of the reference derrick were used with minor changes. The study did not consider redesigning the shape of the derrick and searching for a new conceptual design, which may require changes in drilling and pipe handling equipment.

Due to strict regulations and to finding a conservative proposed stressed skin derrick, only acceptably used material steel was considered in the study. The material is NV-E36, which is high tensile steel with a yield stress of 355 MPA. Choosing steel with a higher yield stress would give a lower weight, but the material costs increase significantly. To be able to use material such as, for instance, composite material, it would have been necessary to perform rigorous studies and tests.

In the reference derrick, there are openings in order to transport out the drilling equipment inside the derrick. In the present study, the openings were ignored because this study is more focused on the global initial design rather than local design. In the detailed study this needs to be considered in order to obtain more accurate result of weight and the thickness of the plate around the openings.

Since in the present study no commercial finite element software was used, local stresses in the structure were based on the previous master's thesis written by Johansson [12], see Appendix B.

1.5 Design criteria

The proposed initial design of a stressed skin derrick was checked against yielding and buckling according to DNV standard rule. The requirements from DNV [9], [10], [11] and [13] and Bassoe technology were the bases for the design criteria in the present study. More detailed information of the chosen design criteria is described in Chapter 5, Section 5.4.2.

The requirements from Bassoe technology for the proposed design are the following:

- The proposed initial design should have the same dimension as the reference derrick with only minor changes without interrupting the drilling operation.

- The analysis and optimization is to be based on a numerical solution using software Matlab [4].

2 Influence of weight on stability

In this chapter, a simple stability calculation was performed to show how an increasing derrick weight influences the stability of the drilling unit.

To illustrate this influence, a simple stability calculation was performed for a typical drill ship with a weight of 8620 mT in lightweight and a vertical centre of gravity of 11.7 m from the keel. The ship was designed by Bassoe technology and all the required data for stability calculation were imported in the stability calculation software Autohydro [14]. The centre of gravity of the derrick in the height direction was estimated to 29.5 m from the top deck of the drill ship. The idea was to increase the weight of the derrick by 10 tons by adding the weight in the centre of gravity of the derrick. The vertical centre of gravity for the system *(Drill ship+ derrick)* is calculated according to the equation (2.1) below.

$$VCG = \frac{X_1 \times Ship_{mass} + X_2 \times derrick_{mass}}{Ship_{mass} + derrick_{mass}} \tag{2.1}$$

where,

$X_1 =$ centre of gravity of ship = 11.7 m (constant)
$X_2 =$ centre of gravity of derrick= 29.5 m (constant)
$Ship_{mass} =$ mass of the drill ship = 8620 mT (constant)

From the equation (2.1), it is observed that an increase in derrick weight means an increase in the vertical centre of gravity for the system. According to ship hydrostatics and a stability book by Biran [15], a floating body is stable if its metacentric height GM lies above its vertical centre of gravity. According to [15], the metacentric height GM is calculated from the equation (2.2), see Figure 2.1 for a definition of the parameters.

$$GM = KB + BM - KG \tag{2.2}$$

where,

$KB =$ Distance from keel to centre of buoyancy, which is approximately $draft/2$
$KG =$ Distance from keel to centre of gravity= VCG in equation (2.1)
$BM =$ Distance from centre of buoyancy to metacentre and calculated according to [12] from equation (2.3).

$$BM = \frac{Ship_{lenght} \times Ship_{breath}^3 / 12}{Ship_{lenght} \times Ship_{breath} \times Ship_{draft}} = \frac{Ship_{breath}^2}{12 * ship_{draft}} \tag{2.3}$$
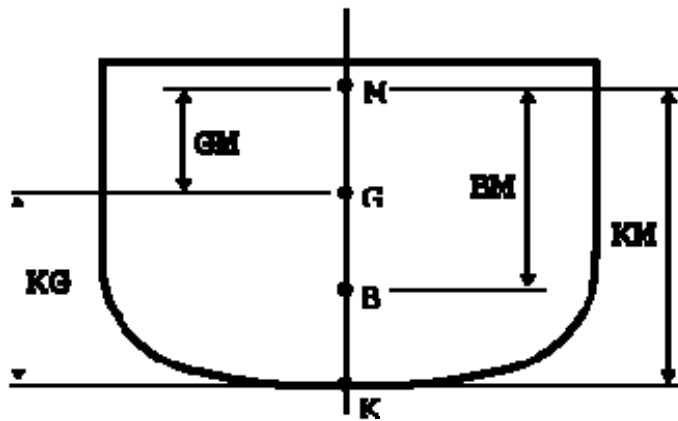
Figure 2.1   Definition of the hydrostatics parameters.

Results calculated in the stability calculation software Autohydro [14] are presented in Table 2.1. In Table 2.1, VCG is defined as the distance from the keel to the vertical centre of gravity for the drilling unit in the example.

Table 2.1   Results of hydrostatic parameters for various derrick weights.

Derrick Mass [mT]	Draft [m]	VCG [m]	GM [m]
510	4.24	12.343	5.734
540	4.26	12.439	5.603
570	4.27	12.537	5.478
600	4.28	12.629	5.349
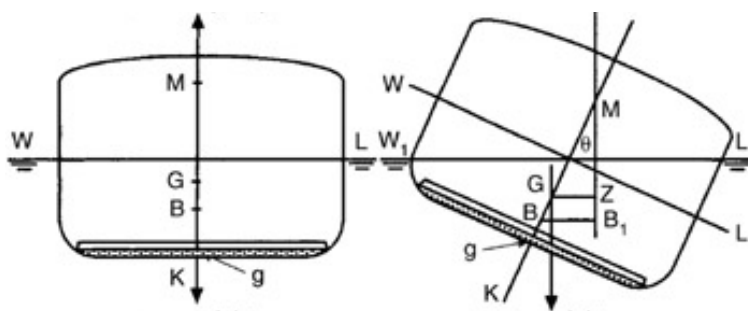
Figure 2.2   Ship in a heeling condition.

Now, assume that the ship heels to starboard by constant angles $\theta = 10°$ as shown in Figure 2.2. The forces of weight and buoyancy produce a righting moment, which is characterized by the righting arm, GZ. GZ is defined as in equation (2.4) according to Biran [15] for a small heel angle.

$$GZ = GM \sin\theta \qquad (2.4)$$

Using the equation (2.4) to calculate GZ with the obtained GM value in Table 2.1 with a constant heel angle of 10°, the result is presented in Table 2.2.

Table 2.2   Results for righting arm for various derrick weights.

Derrick Mass [mT]	GM [m]	GZ [m]
510	5.734	0.9957
540	5.603	0.9730
570	5.478	0.9512
600	5.349	0.9288

The results from Table 2.1 and Table 2.2 are plotted in Figures 2.3 and 2.4 to utilize the effect of an increase in mass of the derrick in VCG and GM.
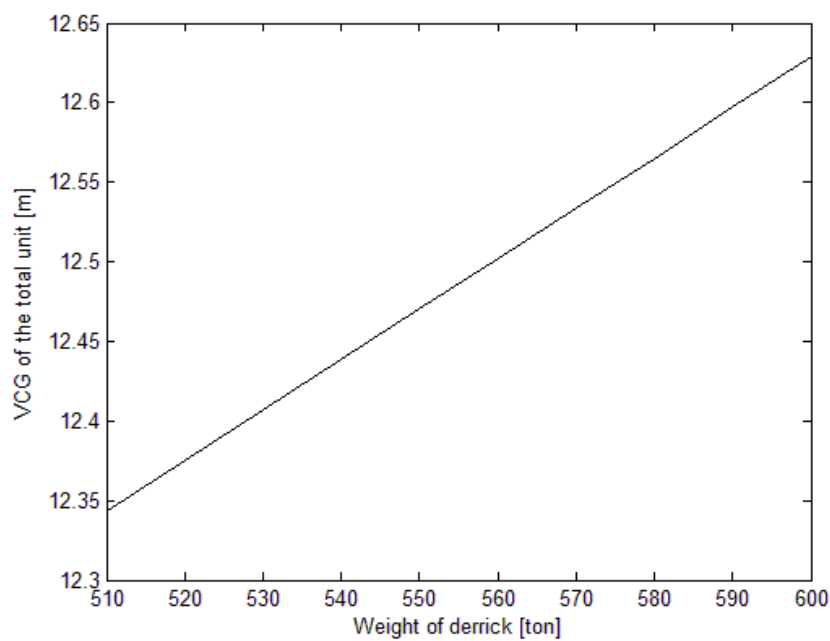
Figure 2.3   Derrick weight influence on the vertical centre of gravity.
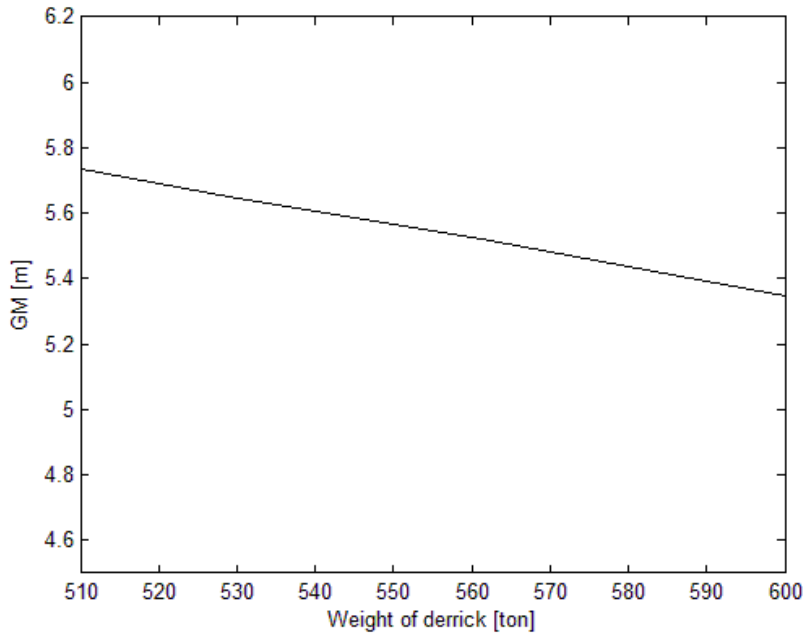
Figure 2.4   Derrick weight influence on GM.

The stability will be more critical if the wind moment is taken into account due to the larger projection area with a protective shell. This will provide a greater heeling moment to the floating unit and the drilling operation is sensitive for a small heel angle, approximately around 4-8°. How large the wind moment increases by introducing a protective shell compared to a truss derrick is presented in Table 2.3. The drag coefficient for a truss derrick according to Gudmestad and Moe [16] should not be less than 0.7, see Figure 2.5. In DNV [13], the drag coefficient for the square section is 2.2 for 0°angle of attack.
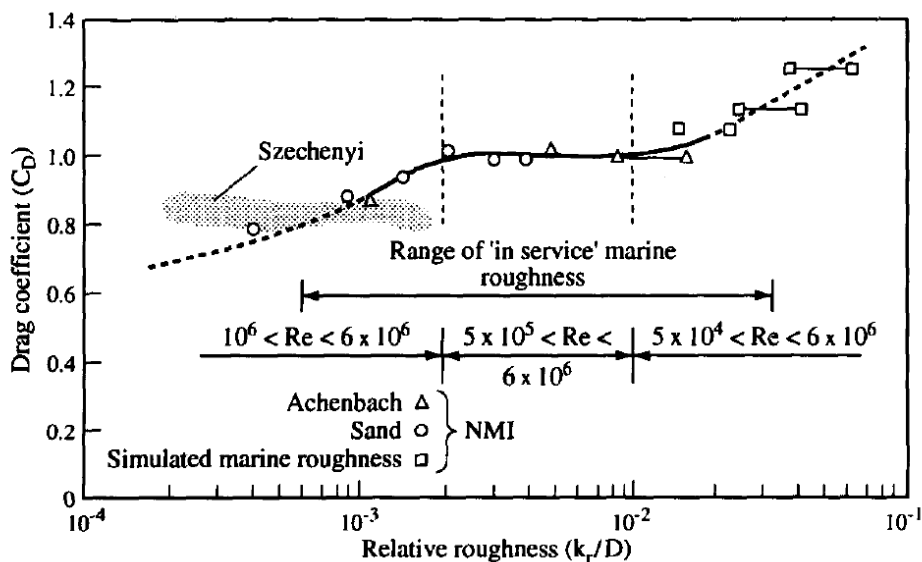
Figure 2.5   Drag coefficient for truss derrick with different surface roughness, from [16].

Table 2.3   *Comparison of wind moment for truss and enclosed derricks.*

	Truss Derrick	**Enclosed Derrick**
Drag coefficient [-]	0.7 (smooth surface)	2.2
Wind moment [kNm]	28	90

To utilize the effect of an increased wind moment, the wind moment was imported to the stability calculation software Autohydro [14]. Unfortunately, the drillship in the example tumbled over with the wind moment due to the fact that the dimensions of the ship in this example were relatively small compared to the derrick size. This example illustrates the sensitivity of stability of offshore units with a covered stressed skin derrick with a high structural weight.

3 Description of the reference derrick

This section presents a structural description of the reference derrick together with the main dimension and all the heaviest equipment of the drilling unit and pipe handling for a drilling operation.

The reference truss derrick was designed by Aker MH [3] and formed the basis for the new design of derrick with regard to choosing equipment, shape, dimensions and force calculations. See Figure 3.1 for all main sections, drilling and pipe-handling equipment. There is a great demand for the selected derrick in the offshore industry due to the following features:

- It accommodates a large area for the storing of drill pipes and casing, which is preferred for offshore units in a drilling operation. The drill string, which is built up by several sub-parts, can be drawn back inside the derrick without being broken into parts and transported out on the pipe rack deck.

- The derrick offers multitasking operation. It can build up stands for the drilling of pipes or casing simultaneously with performing drilling operations. This means that the derrick is the type of one and a half activity (compared to single activity or dual activity).

The main dimension and the capabilities of the derrick are presented in the Table 3.1. In Table 3.1, the term hook load stands for the maximum weight in static conditions that the derrick substructures can withstand, and setback stands for pipe-handling capability and capacity, which stands inside the derrick.

Table 3.1   Dimensions and the capabilities of the reference derrick.

Description	Value
Height [m]	63.5
Base dimension [m]	14 x 15.85
Main structure weight [mT]	390
Hook load [mT]	908
Setback [mT]	986

The derrick is located on the drill floor. Equipment description and weights are taken from the previous master's thesis by Johansson [12]. In the previous study, the equipment weight list did not take into account the equipment weight lower than 4 mT in order to simplify the FE-model analysis. This weight contributes to approximately 2 % of the total structural weight. In the present study, no FE-analysis was carried and to make the optimization study more accurate, an additional weight of 2% was added to the total structure weight. All main equipment, including the associated equipment, is described briefly in Table 3.2 and utilized in Figure 3.1. Also, the total weight of each main part and the location of the equipment in the derrick structure is presented in Table 3.2.
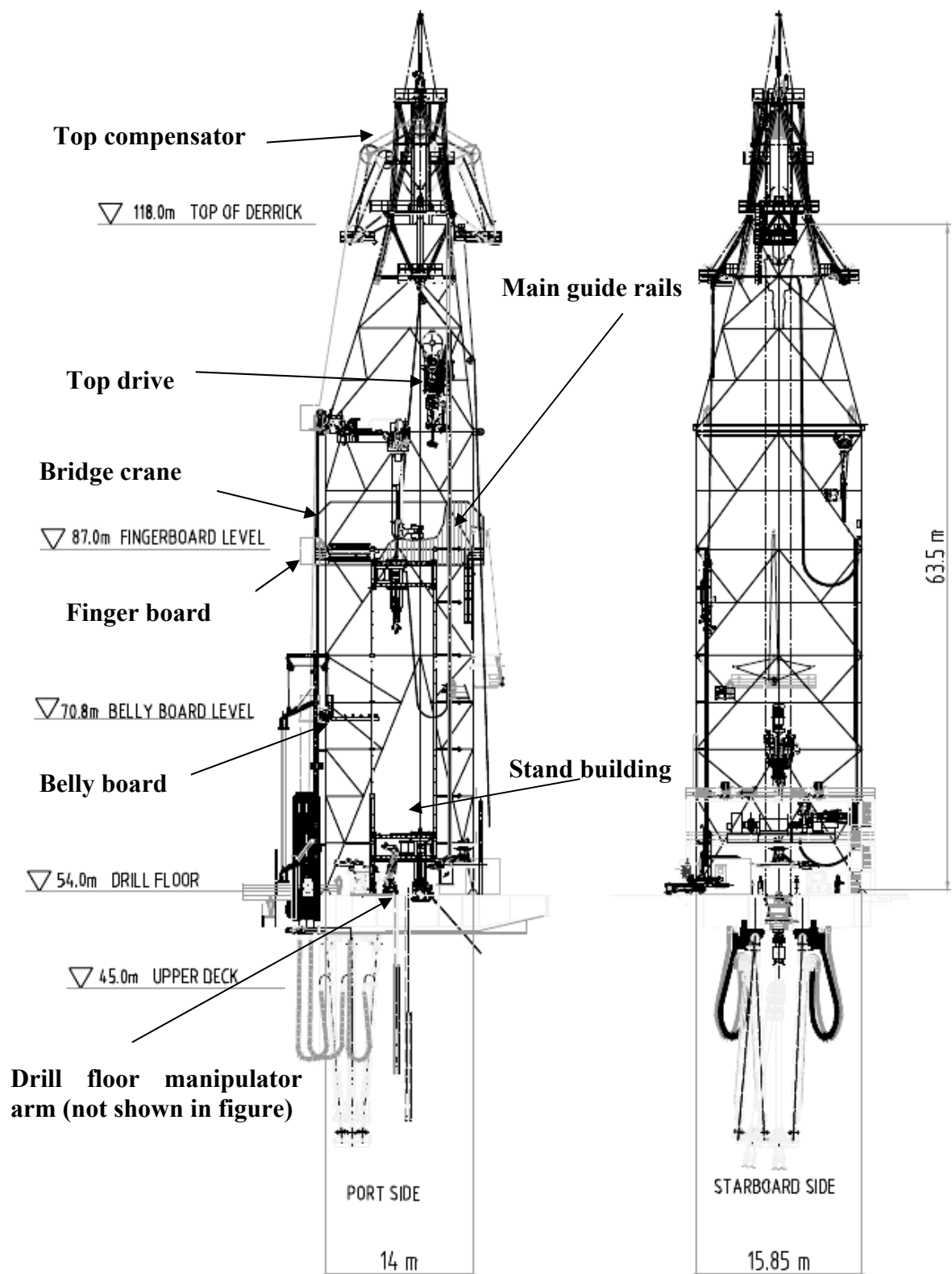
Figure 3.1   Reference derrick with dimensions and heaviest equipment.

Table 3.2   Equipment description of the derrick with weight and location.

Equipment Include supported component	Description	Total weight [mT]	Location
Top compensator	Prevent the rig's motions during the drilling operations. Support to keep the drilling bit in the bottom of the hole	146	Top of the derrick 63.5-58 [m]
Top drive assembly	Hold the drill string and to rotate it during drilling operation. Movable from top to bottom of the derrick	82	Below the top compensator
Main guide rails	Support the top drive. The interference between the top drive and main derrick structure. Located on top to bottom of the derrick	38	Starboard side
Finger board	Top storage area for drilling pipe. 33m above the drilling floor	25	Port side
Belly board	Storage area for drilling pipe. 15.5m above the drilling floor	24	Port side
Bridge crane assembly	Runway for pipe-handling system	45	44m above the drill floor
Stand building assembly	Supports the horizontal and vertical movement of the drill pipes	21	Opening on the aft side
Drill floor manipulator arm	Guides the drilling riser	8	Bottom level
Bulk weights	All other necessary equipment such as cables, pipes, grating, platforms, ladders, handrails and equipment	141	over entire derrick structure

In Table 3.3, a summation of the weights is presented.

Table 3.3   *Weight summation of the equipment.*

Description	Value [mT]
Total equipment weights	530
Main structure weight	390
2 % of additional weight	18.4
Total	**938.4**

For the calculation of the force on the structure due to rig acceleration, the equipment weight was added to the structure weight in the specific position in the height direction as point load. Bulk weights and weight of main guide rails were distributed over the entire derrick structure. The top drive weight location varies over the entire derrick structure depending on the actual position. For the calculation of the force, the critical position of the top drive was assumed, namely at the top of the derrick.

4 Loadings acting on derrick structure

In Section 4.1, a brief description of load cases during operational conditions are described and utilized. In Section 4.2, different types of loads acting on the derrick structure under operational conditions are discussed extensively. Further, the governing loads conditions for the proposed design of derrick is presented in detail. In Section 4.3.1, the drag coefficient for a large Reynolds number and the effect of wind forces and are discussed. In Section 4.3.2, the benefits of a derrick structure with rounded corners instead of the reference derrick are discussed.

4.1 Description of loading condition

A maximum combination of environmental and functional loads was analysed in three different wind and wave directions: head sea, quart sea and beam sea are illustrated in Figure 4.1. This occurs due to the shape of the reference derrick. The loads were also analysed in the opposite directions of the derrick in all directions. The load directions shown in Figure 4.1 are even presented in Table 4.1 with loads and respective acceleration.
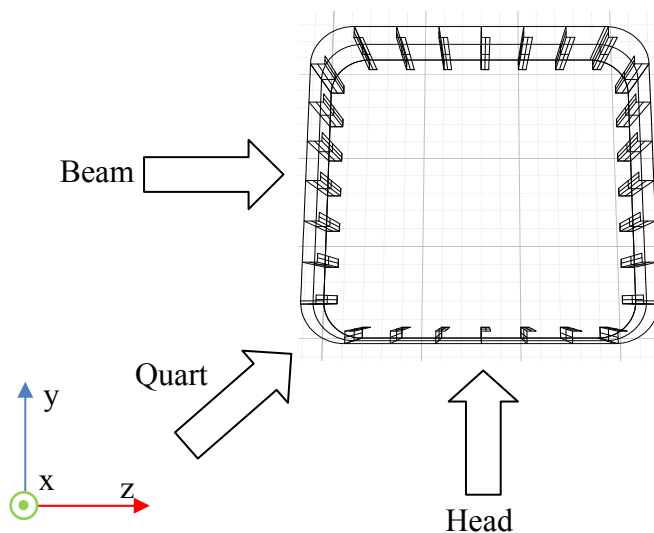
Figure 4.1   Top view of cross section; wind loads in three different study cases.

Loads in Table 4.1 are taken from the Aker MH [3]. The acceleration of the rig and the influence on the derrick is given in [3] for both the top and bottom of the derrick for three different wind and wave directions. For simplicity, only the highest values for accelerations were used.

Table 4.1   Designing load conditions for the proposed design of derrick.

Loading condition			
Loads	**Operational head sea**	**Operational quart sea**	**Operational beam sea**
Hook load [mT]	908		
Setback	986		
Wind U(10m,60s) [m/s]	36		
Longitudinal acceleration [m/s^2]	3.29	2.69	0.1
Transverse acceleration [m/s^2]	0.1	2.47	4.17
Vertical acceleration [m/s^2]	0.87	0.92	1.01

4.2 Types of loads

The reaction-force analyses of the derrick structure were carried out for different types of loads. A brief definition and description of all load types is described in sub-chapters below.

4.2.1 Permanent loads and variable functional loads

The permanent loads are the total weight of the structure including all secondary steel, fixed equipment and other accessories that were shown in Table 3.3. These loads are considered as being constant in all design conditions. Variable functional loads present the loads due to the drilling operation, hook load and setback. Different structure parts are influenced from the operational load, which is described in Sections 4.2.2 and 4.2.3

4.2.2 Wave loads

The wave-induced loads on the derrick structure are considered in Sections 4.2.3 and 4.2.4 with reference to the acceleration of the rig.

4.2.3 Hook Load

The top drive is supported by horizontal main guide rails and therefore the hook load influences the main guide rails. In Table 4.2, the resulting forces of the hook load due to gravity and accelerations of the rig are shown. The value is computed by taking the hook load of 908 mT and multiplying the acceleration values in Table 4.1. In the vertical direction, the gravity acceleration of 9.81 m/s^2 was added in order to get the resultant force of the hook load in the vertical direction. To calculate the transversal forces of the hook load to the derrick structure, the critical position of the hook load was assumed to be 10 m from the top of the derrick.

Table 4.2   Hook load due to the acceleration of the rig.

Hook Loads (908mT) due to acceleration of the rig			
Loads on derrick component	**Operational head sea**	**Operational quart sea**	**Operational beam sea**
Hook load the vertical direction [kN]	9697	9743	9825
Main guide rails Longitudinal direction [kN]	2987	2443	91
Main guide rails Longitudinal direction [kN]	91	2243	3786

4.2.4 Setback

Setback is supported vertically by the drill floor, belly board and fingerboard. Regarding the transversal force absorption of the setback, one assumption was made. One-fourth of the inertia force is taken up by the drill floor and fingerboard, respectively (246.5 mT), and half of the force is taken up by the belly board (493 mT). In the present study, the drill floor was not a part of the weight optimization and the forces on the drill floor were not considered. The resulting force of the setback due to acceleration is presented in Table 4.3.

Table 4.3   Setback load due to the acceleration of the rig.

Setback (986 mT) due to acceleration of the rig			
Loads on derrick component	**Operational head sea**	**Operational quart sea**	**Operational beam sea**
Fingerboard longitudinal direction [kN]	811	663	25
Fingerboard transverse direction [kN]	25	609	1028
Belly board longitudinal direction [kN]	1622	1326	49
Belly board transverse direction [kN]	49	1218	2056

4.3 Wind loads

As mentioned in Chapter 2, Section 2.1, one has seen how the wind moment increased significantly with a protective shell compared to a truss derrick. Here, in Sections 4.3.1 and 4.3.2, a background and how to decrease wind force is presented in detail.

4.3.1 Background and research on C_d

To analyse the wind loads, the drag coefficient is a parameter that needs to be obtained. A study was made in different literature on the subject in order to see how the drag coefficient decreases with rounded corners for a different radius on a square shape for a high Reynolds number.

Today, there are no valid data and experimental results to determine the drag coefficient for a square section with various corners for a high Reynolds number ($4x10^7$). There is an analytical investigation and evaluations made by Richter [17] on wind forces for square sections with various corners, but the study only covers the Reynolds number in the range of 10^3 and $3x10^5$. Some search was made in the scientific web to find relevant research in the area. Most articles and evaluations were found for high-rise building with a square shape. According to Zheng and Zhang [18], the Reynolds number would have a small influence on the flow field and mean pressure coefficient on the high-rise building if the Reynolds number is greater than $1x10^4$. This has also been mentioned by Zhou et.al [19].

In the wind loading of the structure book by Holmes [20], Figure 4.2 shows how the drag coefficient for a square body with rounded corners decreases with the increasing Reynolds number for a certain radius. In the transition area, where the boundary layer from laminar to turbulent occurs around the Reynolds number of 10^4-10^5, there is an extreme decrease in the drag coefficient and a slight increase again in the turbulent region and stabilization around a specific value. However, this value of drag coefficient will never exceed the value of the laminar region around 10^4-10^5. This was also confirmed by a discussion with the research group Hydrodynamics at Chalmers University. This means that the value given in the report of the investigation and evaluations made by Richter [17] on wind forces for square sections with various corners is valid and conservative, but with a safety margin on wind loads. The effect of the turbulent intensity on the drag coefficient is also mentioned in the report and due to a higher turbulent intensity at sea, a safety margin in the wind loads is desired in order to ensure the safety of the derrick structure.
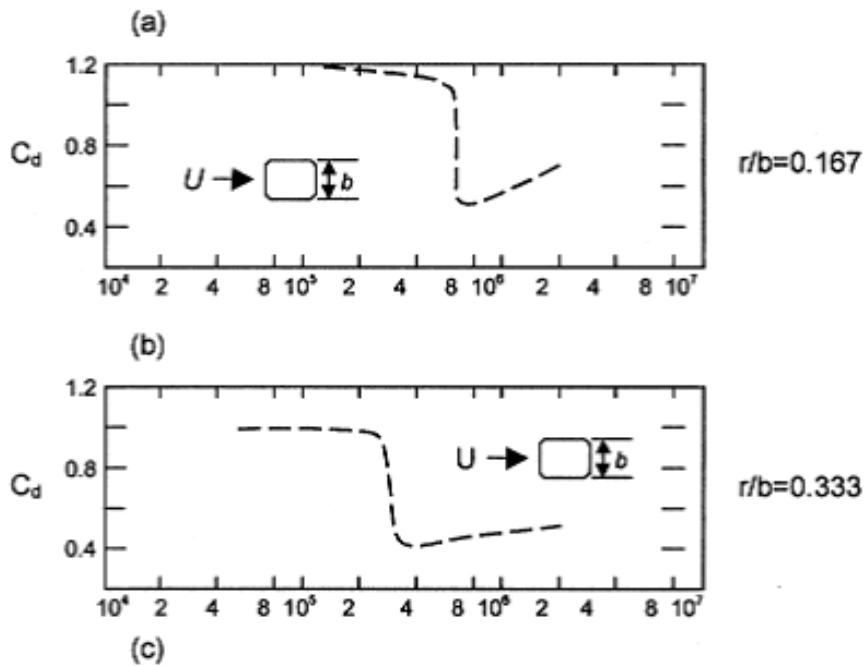
Figure 4.2   Decreasing drag coefficient with an increasing Reynolds number for two different radius ratios, from [19].

The effect of the Reynolds number on the drag coefficient is not subsequently considered. To compare the drag coefficient [17] with DNV [13], there are slightly little deferens between the drag coefficient values. In [17], the values are approximately 2 % higher than DNV [13]. For further analysis, the Richter investigation [17] will be used for obtaining the drag coefficient.

4.3.2 The effect of rounded corners on wind force

The influence of a corner radius on the drag coefficient was observed at an early stage by Scruton in the Holmes literature [20]. In Richter [17], investigatory wind model tests were performed on models with a different radius. The result of the investigation is presented in Tables 4.4-4.6 and Figures 4.3-4.5 for an attack angle of $0°$, $45°$ and $90°$ of wind direction. R/W is the ratio of the corner radius to the width of the reference derrick (W=15.85 and W=14 m). The values in the tables are for the Reynolds number of $2x10^5$.

Table 4.4   Drag coefficient of 0° angle of attack for different corner radii (plur. av radius).

C_d for 0° angle of attack (W=15.85 m)		
Radius [m]	**Radius ratio R/W [-]**	**C_d [-]**
0	0	**2.17**
0.6	0.037	**1.86**
1.2	0.076	**1.614**
1.8	0.113	**1.43**
2.4	0.151	**1.29**
3	0.189	**1.184**
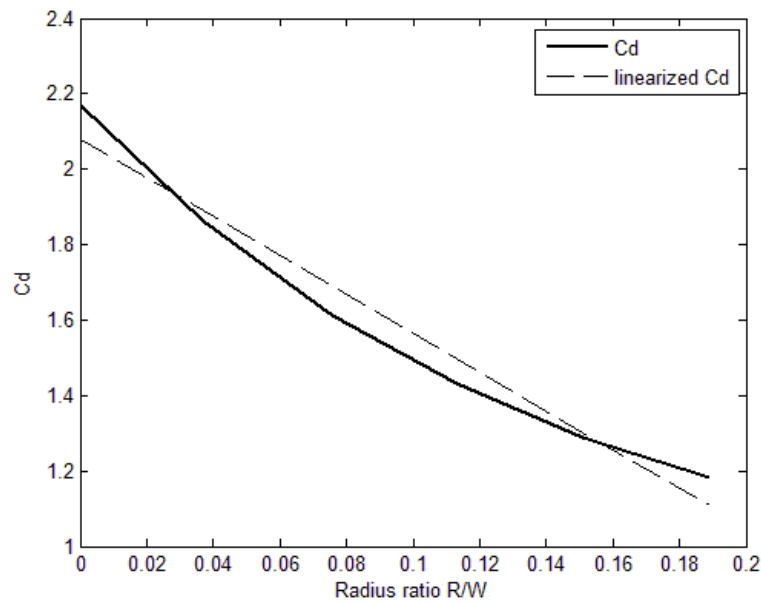
Figure 4.3   Drag coefficient of 0° angle of attack for different corner radii.

Table 4.5   Drag coefficient of 45° angle of attack for different corner radii.

C_d for 45° angle of attack (W=15.85 m)		
Radius [m]	**Radius ratio R/W [-]**	**C_d [-]**
0	0	**2.195**
0.6	0.037	**2.161**
1.2	0.075	**2.128**
1.8	0.114	**2.087**
2.4	0.151	**2.032**
3	0.189	**1.98**
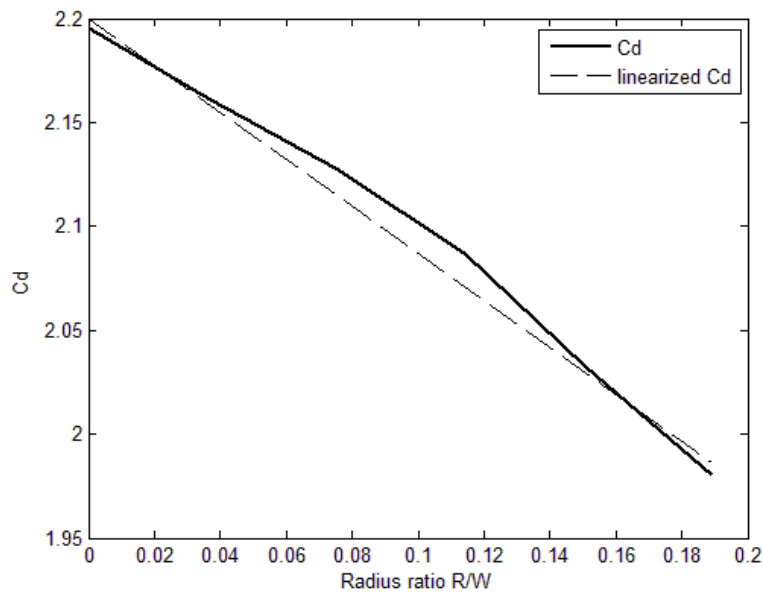
Figure 4.4   Drag coefficient of 45° angle of attack for different corner radii.

Table 4.6   Drag coefficient of 90° angle of attack for different corner radii.

C_d for 90° angle of attack (W=14 m)		
Radius [m]	**Radius ratio R/W [-]**	**C_d [-]**
0	0	2.17
0.6	0.042	1.838
1.2	0.085	1.5748
1.8	0.128	1.4064
2.4	0.171	1.236
3	0.214	1.12
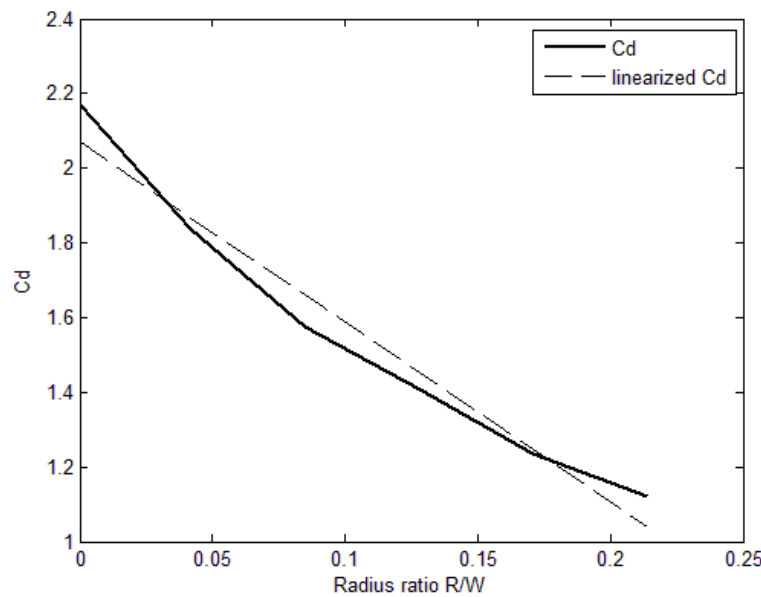
Figure 4.5   Drag coefficient of 90° angle of attack for different corner radii.

For the linear equations in Figures 4.3-4.5, a determination coefficient R^2 was calculated. According to Newbold el.at [21], the determination coefficient R^2 explains how many per cent of the variation in C_d can be explained by R/W. A rule of thumb in statistics is that if the determination coefficient is larger than 0.64, there is a strong relationship between x and y. The linear equations in Figures 4.3-4.5 had a determination coefficient greater than 0.96 and using the linear relation equations to predict the C_d for the desired R/W is a good approximation.

The largest possible corner radius allowed without interference from the drilling operation is 2 m up to the height of 43.65 m. Above this height a larger radius of approximately 3 m can be obtained without interference from the drilling equipment. Considering the limitation of space, the drag coefficients were computed with the

linear equations in Figures 4.3-4.5 for different wind directions. The result is presented in Table 4.7.

Table 4.7   The drag coefficient used in the study.

Drag coefficient C_d			
R [m]	0°	45°	90°
0	2.2	2.4	2.2
2	1.43	2.05	1.38
3	1.10	1.98	1.05

4.3.3 Wind force calculation

The designed wind speed for operational conditions used in the current study was taken from the Aker MH [3], see Table 4.1. This value is for a height of 10 m above the sea level with an average time of 1 minute. According to DNV [13], this wind speed is often referred to as *sustained* wind speed.

To obtain the wind velocity at a certain height and the desired average period, the expression in [13] was used, see Equation (4.1). This expression converts mean wind speeds between different average periods. If the average period of wind velocity in the expression is $T < T_{60s}$, the expression provides the most likely largest mean wind speed over the specified average period *T*.

$$U(T,z) = U_{(10m,60s)}\left(1 + 0.137\ln\left(\frac{z}{H_{10m}}\right) - 0.047\ln\left(\frac{T}{T_{60s}}\right)\right)$$
(4.1)

where,

$z =$ height of interested
$H_{10m} =$ reference height (10m)
$T =$ average period of interest
$T_{60s} =$ reference average period (60s)
$U_{(10m,60s)} =$ wind speed at the reference height and reference average time (36 m/s)

With these wind speeds, the basic wind pressure was calculated, from equation (4.2).

$$q = \frac{1}{2}U_{(T,z)}^2 \rho_a$$
(4.2)

where,

$\rho_a =$ mass density of air (1.226 kg/m^3) for dry air at 15°C

Figure 4.6 presents the increment of wind pressure dependent on the height above the sea level due to the higher wind velocity.

Figure 4.6   Wind pressure along the derrick height.

The wind force acting on the derrick structure normal to the surface was computed according to Equation (4.3).

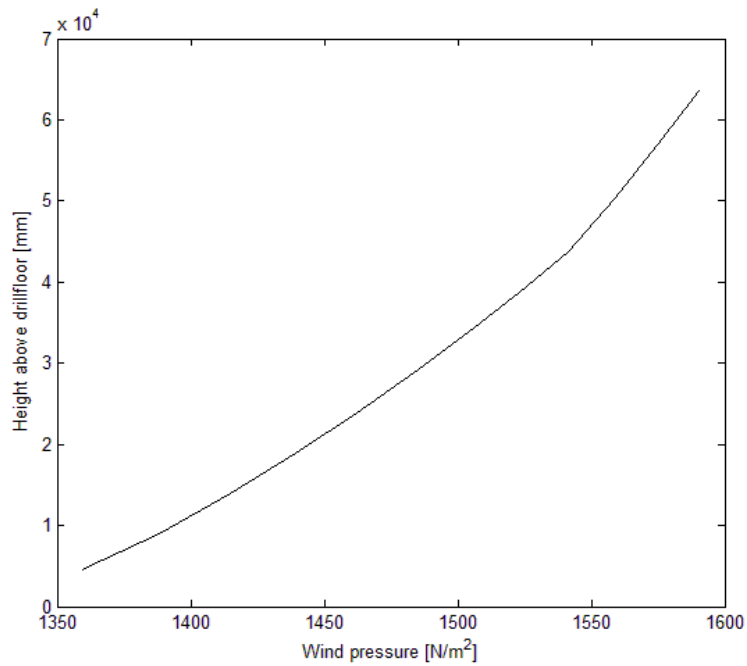$$F_W = C_d \cdot q \cdot S \cdot \sin \alpha$$

(4.3)

where,

C_d = drag coefficient
q = basic wind pressure
S = projected area of the member normal to the direction of force
α = angle of attack

5 Design criteria for a stressed skin derrick

The design of derrick should be according to DNV offshore standard rule. In Section 5.1, a comparison between two design philosophies is discussed together with a brief description about the chosen philosophy. The most important design criteria in DNV [9], [10], and [11] are presented in this chapter. In Section 5.2, buckling modes and yielding of stiffened plate are described in general as well as possible failure modes in the structure. In Section 5.3, yielding and requirements from DNV are presented. In Section 5.4, an introduction of buckling and yielding check software STILPA [7], [8] is described.

5.1 Design methods, WSD vs. LRFD

The design of the structural details of the stressed skin derrick required a definition of the design methods that have been widely used in offshore structures, namely Working Stress Design (WSD) and Load and Resistance Factor Design (LRFD) criteria. The chosen method in the current study was WSD [9].

The difference between WSD and LRFD is in the calculation of uncertainties in the design and how to compensate for this in the design. The uncertainties in LRFD methods are divided into two safety factors: nominal capacities (γ_M) and the resistance factor (γ_F). Nominal capacities account for uncertainties in variable material properties, construction and tolerance. The resistance factor takes into account uncertainties in the design load. In the WSD method, a single safety factor, the usage factor (η_p), is used which handles both uncertainty in the load and capacity of material according to Bulleit [22].

The LRFD method offers a better ability to handle certain sources of uncertainty but requires broad statistical data on the variation of loads and material compared to WSD. However, WSD is easier to use and utilize due to fewer factors by using the actual load and material properties according to Bulleit [22]. For this reason, the design of derrick was based on the WSD method [9].

5.1.1 WSD-working stress design criteria

In the WSD method, different load conditions are analysed and the calculated results are compared against the highest permissible stresses. The permissible stress in DNV [9] is defined by a safety factor, called usage factor η_p. The usage factor η_p is calculated from Equation (5.1) by multiplying the basic usage factor η_0, which depends on the loading condition, see Table 5.1 and a characteristic strength of the material. The structural member should be designed against the worst case of the loading condition. The load conditions are presented in Table 5.1 taken from DNV [9].

$$\eta_p = \eta_0 \cdot \beta \tag{5.1}$$

where,

η_p = usage factor; β = characteristic strength of the material; η_0 = basic usage factor

Table 5.1   Usage factor η₀ for different load conditions for buckling and yielding.

Case	*Description*	*η₀*
a)	Functional loads	0.6
b)	Maximum combination of environmental loads and associated functional loads	0.8
c)	Accidental loads and associated functional loads	1.0
d)	Annual most probable value of environmental loads and associated functional loads after credible failures, or after accidental events	1.0
e)	Annual most probable value of environmental loads and associated functional loads in a heeled condition corresponding to accidental flooding	1.0

The governing loading condition in the present study was *case b)* in Table 5.1 for the design of stressed skin derrick. The coefficient β according to DNV [9], should be equal to one in both the yielding and buckling mode. The permissible stress is calculated according to Equation (5.2)

$$\sigma_{permissible} = \eta_0 \cdot \beta \cdot \sigma_{yielding} = 0.8 \cdot 1 \cdot \sigma_{yielding}$$

(5.2)

It was important to clarify which geometrical parameters had the most influence on buckling and yielding, but also for optimization of the derrick with regard to weight. In Table 5.2, a summation of all parameters and the possibility to optimize the specifics are explained.

Table 5.2   Parameters of importance for optimization and strength of the derrick.

Design Parameters of derrick structure	Optimization possibility to reduce mass and the importance for buckling & yielding
Permanent loads from equipment	Constant
Functional load	Decrease by reducing the mass
Material yielding stress	Constant in the initial design for a chosen material
Thickness of plate	Important for mass, buckling and yielding
Dimension of stiffeners and stringer	Important for mass, buckling and yielding
Spacing of stiffeners and stringer	Important for mass, buckling and yielding
Restraint coefficient	Constant according to DNV standard

The material chosen for the design was high tensile steel NV-E36 with a yielding stress of 355 MPa [9]. The permissible stress calculated from Equation (5.2) to 284 MPa. This means that all stress components and the von Mises stress in the design should not exceed 284 MPa, and for buckling the usage factor must be lower than 0.8.

The von Mises equivalent stresses is computed according to Equation (5.3).

$$\sigma_{vM} = \sqrt{\sigma^2_x - \sigma_x\sigma_y + \sigma^2_y + 3\tau_{xy}^2} \tag{5.3}$$

where,

σ_x = axial stress

σ_y = transversal stress

τ_{xy} = shear stress between stiffened plates

5.2 Buckling and yielding

Buckling and yielding were undoubtedly the two design criteria in the study of this kind of offshore structure. According to Stamatelos el.al [23], there are several critical failure modes for a stiffened plate that needs to be verified and checked when the plate is subjected to a compressive load. In Figure 5.1, a stiffened plate with structural members under a compressive load is utilized.
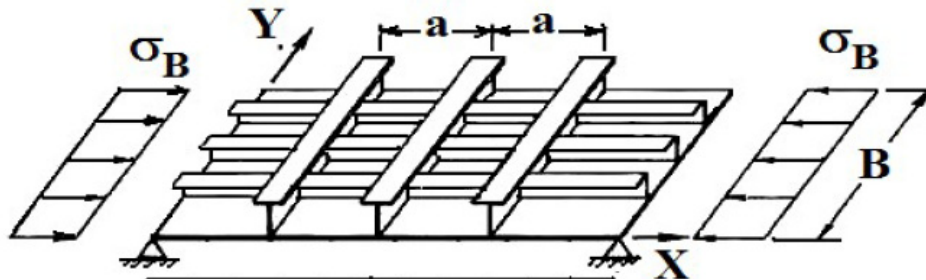
Figure 5.1 Stiffened plate in both the longitudinal and transverse directions under a compressive load.

A buckling and yielding check of the structure was performed by using DNV [9] and [11]. The recommendations and equations in DNV [9] and [11] apply to plate, stiffeners and girders. The following buckling and yielding analysis must be performed for a stiffened plate according to DNV [9] and Ringsberg [24].

1) Plate between the supports (*local buckling*)

2) Buckling of longitudinal stiffeners

- Check lateral buckling (Euler buckling)
- Check Torsional buckling
- Buckling of the web plate of the stiffener
- Buckling of the flange of the stiffener

3) The transverse beam strength beam is larger than required, otherwise the entire plate may buckle.

4) Yielding check of plate, stiffeners and girders.

The possible failure modes for a stiffened plate are utilized in Table 5.3 in general. Table 5.3 only describes failure modes for plate and stiffener and similar phenomena occur for girders when a plate is subjected to compressive loads.

The buckling and yielding check was done by using software STIPLA [7], [8] developed by *StruProg* with implemented DNV rules to ensure the safety of a stressed skin derrick against possible failure modes. For a more detailed description about the software, see Section 5.4.

Table 5.3   Failure modes of a stiffened plate under compressive loads summarized from [23].

Failure mode of buckling/yielding	Description
Mode 1	The global buckling mode of plate-stiffeners. This mode usually occurs when the ratio of the stiffeners to the plate stiffness $EI_{stiffener} / BEI_{plate}$ is relatively small. B is the width of the plate
Mode 2	Local buckling of the plate segment between the stiffeners. This mode leads to plate collapse due to local buckling and consequent yielding of the plate segment between stiffeners
Mode 3	Combined buckling of the stiffener and plate. This mode occurs when the stiffeners are not torsionally rigid enough. If the stiffener is stiff enough the buckling mode is similar to mode 2.
Mode 4	Local buckling of the stiffener web; this mode usually occurs due to lateral deformation of the face plate.
Mode 5	Lateral torsional buckling of the stiffener web, which is similar to mode 4 except that the buckling of the stiffener is a lateral torsional buckling. This mode occurs when the ratio of stiffener web height to stiffener web thickness is too large. This mode can also cause a global buckling mode to follow immediately.
Mode 6	Yielding at the corners of the plate between stiffeners, which is usually termed a plate-induced failure at the ends. This type of mode occurs when the panel is predominantly subjected to biaxial compressive loads
Mode 7	Yielding of the plate stiffener combination at the mid-span, which is usually termed a plate-induced failure at the mid-span.
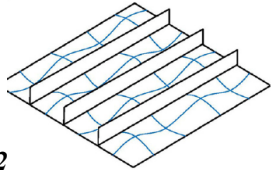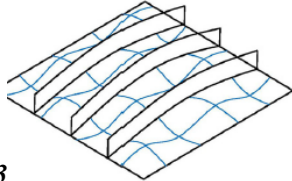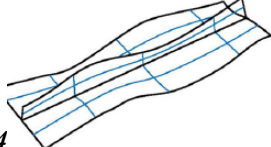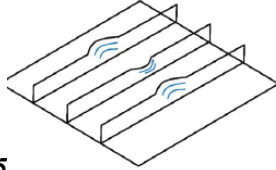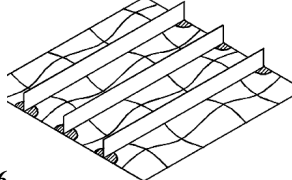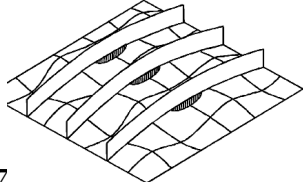
5.3 Yielding check

According to DNV [9], there is a requirement for a minimum scantling thickness for a plate, stiffened panels, web and flange with respect to yielding. The minimum required thickness t is calculated according to Equation (5.4) from [9]

$$t = 15.3 \frac{t_m}{\sqrt{\sigma_{yeilding}}}(mm) = 15.3 \frac{7}{\sqrt{355}} \approx 6mm \tag{5.4}$$

where,

t_m = 7 mm for primary structural elements and 5 mm secondary elements

$\sigma_{yeilding}$ = Minimum yielding stress for design material

DNV [9] contains formulas for the required minimum thickness and minimum section modulus of the stiffeners due to lateral pressure. In the present study, there are low wind pressures as lateral pressure. The required thickness was checked according to the formula in [9]. The result showed an extremely low thickness requirement compare to 6 mm. This criterion was not the governing design criteria and was not considered.

In a further study and analysis, the thicknesses of all structural members will not be less than the calculated thickness in Equation (5.4) and this leads to the conclusion that buckling is the governing design criteria and yielding does not occur before buckling. This conclusion is verified later in Chapter 9, Section 9.3 after the optimization.

5.4 Buckling and yielding check by software STIPLA

STIPLA is developed by StruProg, 2012 [7], [8] with implemented DNV rules for verifying the buckling and yielding of plate, stiffener and stringer/girder. The program is based on the following DNV documents:

- DNV-OS-C201 [9]
- DNV-RP-C201 [10]
- DNV-OS-C101 [11]

STIPLA is sub-divided into four main categories. In the present study, the following categories in STIPLA were used: DNVRPG [7] and DNVRPS [8]. DNVRPG is for the buckling and yielding check of stringer/girders and DNVRPS is for stiffeners and plate. Both software programs are based on LRFD and WSD design philosophies, which are described in Section 5.1. As mentioned in Section 5.1.1, the design methodology used in the current study was WSD [9].

For a buckling and yielding check of all structural elements, STIPLA calculates a usage factor according to DNV [9], [10] and [11] for all possible failure modes in the structure. The usage factor is defined as utilized material strength against buckling and yielding, respectively. The safety factor defines the safety of structure elements against the failure mode. Bassoe technology complies with DNV rules and does not

introduce an additional safety margin for the structures. Furthermore, the safety factor for a derrick design in the present study is defined as the inverse of the usage factor. The design criteria in the present study against buckling and yielding can be summarized as follows:

- All usage factors against failure modes calculated in STIPLA DNVRPG [7] and DNVRPS [8] must be ≤ 0.8

- The safety factor for structural elements must be ≥ 1.25

- The equivalent von Mises stresses for the structure elements must be ≤ 284 MPa

All usage factors calculated in STIPLA and the definition of these are described in Sections 5.4.1 and 5.4.2. The derivations of the usage factors from DNV rules are described in the STIPLA DNVRPS manual [25] and the STIPLA DNVRPG manual [26].

5.4.1 DNVRPS *(the WSD method)* for stiffener and plate

The buckling and yielding of stiffener and plate was performed in STIPLA DNVRPS [8]. In Table 5.4, all usage factors are utilized with reference to DNV rules.

Table 5.4   Usage factors for plate and stiffener from DNVRPS [8].

Usage factor	Definition	Reference to DNV rules
UF_{plate}	Plate lateral capacity check	DNV-RP-C201 [5]
UF_t	Minimum thickness control	DNV-OS-C201 [8]
UF_{zp}	Minimum section modulus, plate side	DNV-OS-C201 [8]
UF_{zs}	Minimum section modulus, stiffener side	DNV-OS-C201 [8]
UF_V	Stiffener shear capacity check	DNV-OS-C201 [8]
UF_p	Plate buckling check	DNV-OS-C201 [8]
UF_s	Stiffener buckling check at end and mid span	DNV-OS-C201 [8]
UF_{yp}	Plate yielding check	DNV-OS-C201 [8]
UF_{ys}	Stiffener yielding check	DNV-OS-C201 [8]

5.4.2 DNVRPG *(the WSD method)* for stringer/girder

The buckling and yielding check of girder/stringer was performed in DNVRPG [7]. In Table 5.5, all usage factors are utilized with reference to DNV rules.

Table 5.5   Usage factors for plate and stiffener from DNVRPS [7].

Usage factor	Definition	Reference to DNV rules
UF_g	Girder buckling check at end and mid-span	DNV-OS-C201 [8]
UF_p	Plate buckling check	DNV-OS-C201 [8]
UF_{lv}	Girder shear control	DNV-OS-C201 [8]
UF_{zg}	Minimum section modulus check for girder	DNV-OS-C201 [8]
UF_A	Girder web-area control	DNV-OS-C201 [8]
UF_{yg}	Girder yielding check	DNV-OS-C201 [8]

6 Description of the new derrick design

In the present chapter, a description and idea about the proposed design is explained. In Section 6.1, the minor changes in the design of reference derrick are explained as well as a description of the current design with regard to beam shape, dimensions variation and thickness of outer plate. In Section 6.2, the additional weight due to welding is explained and calculated.

6.1 Design description

The design of the derrick as a construction met with a number of limitations. Due to the stability sensitivity caused by the heeling, the derrick contribution of elevated centre of gravity was limited. This means that the weight of the structure material used in the current study was limited. One other issue while designing this kind of construction is that the strength of the wind loads acting on the structures makes the operational environment as one of the most extreme kinds in the seas.

In the current study, there was no purpose to modify the type of the equipment utilized for drilling. Hence, the geometry change of the initial design of the skin derrick was limited for the space needed for operation of the equipment. Also, more oriented studies of optimizations against the weight without amending the breadth, length and height of the derrick were carried out.

The initial design of the derrick in this study arrangement had the equivalent length and breadth at the bottom as the reference truss structure. As was briefly described in Chapter 3, due to the reduction of the drag coefficient factor, the outer shell of the derrick was designed with rounded corners. Because of easier installation in the welding area, the enclosed derrick was not round-shaped at the bottom of the structure up to 9 m. The outer shell was designed with rounded edges with a radius of 2 m at all corners from 9 m up till 43.65 m. The choice of the size of this radius is affected by the limitation of the space required for the drilling equipment.
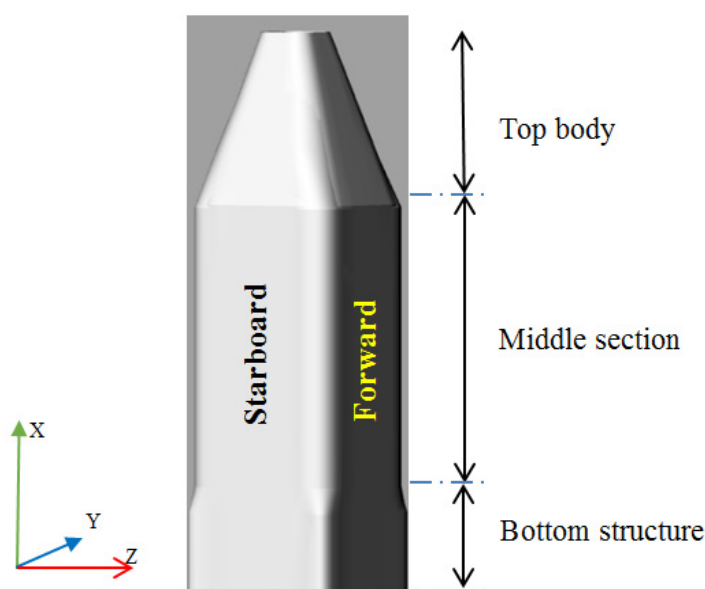
Figure 6.1   Stressed skin derrick with coordinate system in the study.

The highest part of the derrick was also designed with rounded corners. The size of the radius of this part was not limited as much as the part in the middle of the derrick and was increased to 3 metres just at beginning of the folding. This rounded corner was emerged to a sharper radius and the radius at the highest point was reduced to 1.5 m. In order to utilize the shape of derrick, a simple 3D model was created in Rhino 3D [27] to show the initial design of a stressed skin derrick, see Figure 6.1.

The chosen type of stiffener and stringer to stiffen the plate, were L-shaped stiffeners in the longitudinal direction and a T-shaped stringer in the transverse direction, see Figure 6.2. These two shapes are the most commonly used ones in ships and in the offshore industry for making the structure strong enough and capable of resisting the excepted loads with a low weight.
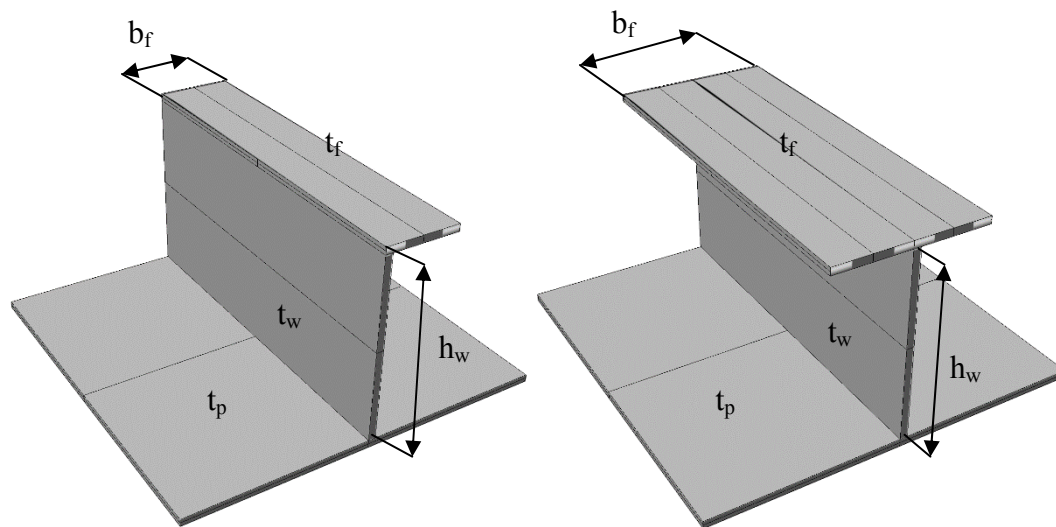
Figure 6.2   L-stiffener and T-stringer used in stressed skin derrick design.

According to Badran el.at [28], the Y-shaped stiffener utilized in Figure 6.3 has a higher ultimate strength failure load and a lower weight compared to a T-shape, if the residual stresses in the beam are not considered. Using a Y-shaped stiffener in ships and offshore structures requires a large space for inspecting the structure during the service life and permits the welding process. In this study and the proposed design, a Y-shape is undesirable due to the limitation in space needed for drilling equipment and operation and requires a more extensive welding process. Due to space limitation and a strict requirement for inspection in the offshore industry, the L and T shapes are the optimum options for stiffening the plate in the derrick.
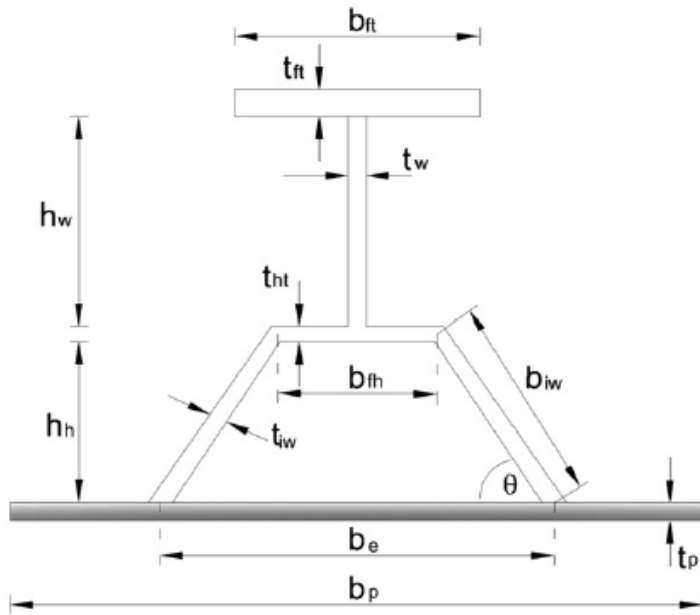
Figure 6.3   Y-shaped beam, from [28].

The thicknesses of the plate varied between the transverse stringer along the height of the derrick in all sides, namely the segments in the vertical direction, see Figure 6.4. The segment number is specified and dependent on the number of stringers used in the stressed skin derrick. The thickness of the plate had a significant impact on both structural weight and strength of derrick. To reduce the weight with the required strength, the sub-division between the stringers was necessary for achieving the optimum weight of the derrick.
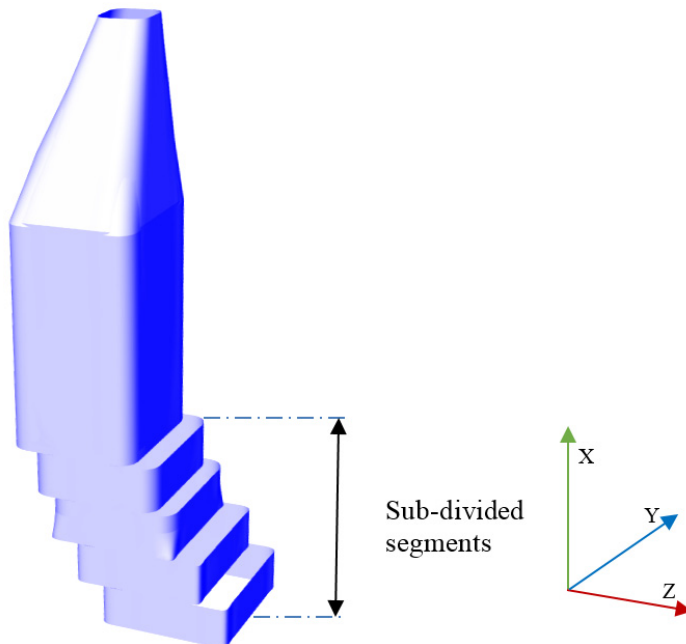
Figure 6.4   Derrick with sub-divided segments in the vertical direction.

The dimension of the longitudinal L-stiffeners also varied along the sub-divided segments. The spacing of the stiffeners was constant in the vertical direction on each side to make the assembly easier. In Figure 6.5, a part of the structural elements inside the derrick are utilized to show the structural elements and arrangement of these.
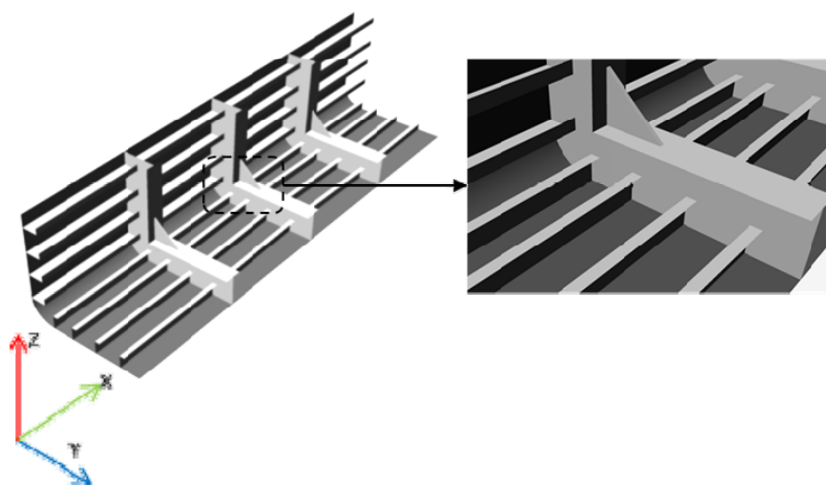
Figure 6.5   Part of the derrick structure utilizing the structural elements used in the proposed design inside the derrick with brackets on right.

The transverse T-stringer spacing and dimensions also varied along the height of the derrick for each of the segments. The spacing in the bottom section of the derrick was less than at the top and middle sections due to a greater global bending moment in the bottom section. The number of stringers had a great impact on the total weight of the structure and on the global buckling of the structure and achieving the proper number of stringers with sufficient strength was the key to keeping the total weight as low as possible. To transfer and distribute the force better in the structure elements, brackets were used at the corners of the stringers, see Figure 6.5. The dimensions of the brackets were dependent on the dimension of stringers in each segment and were obtained when the dimension of the stringers was determined.

To prevent the stringers from lateral torsional buckling, tripping brackets were used between the stiffener support and stringers. The tripping brackets were located on every fourth stiffener. The typical thickness of the tripping brackets used in the offshore structure is 10 mm. In Figure 6.6, the red colour indicates the tripping brackets.
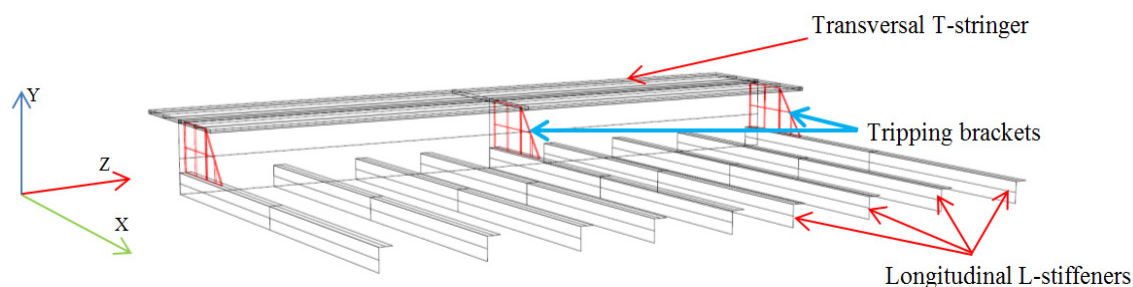
Figure 6.6   Stringer and stiffener with supported tripping brackets in every fourth stiffener indicated with red colour.

6.2 The additional weight of welds

The manufacturing cost of a stress skin derrick is higher than a conventional truss derrick due to the larger joint welding area because of the number of stiffeners and transversal stringers with tripping brackets. Since the reduced weight of the derrick will increase the stability of the oil rig and the drilling crews want to operate under workable conditions, the higher cost will be convincing for the customer.

The welding between the longitudinal and transversal stiffeners is a *fillet welding* and in order to estimate the additional weight of the welding joint to the whole structure, the cross section of the welding was calculated according to Okumoto el.at [29], Figure 6.7.

In Figure 6.7, the parameter is estimated and defined according to [29] as $w = 0.165t$ and $l = 0.233t$, where t is the thickness of the web of the stiffeners.

The calculated additional weight of the weld joint was approximately 21 tons.
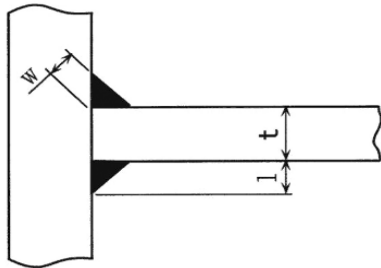
Figure 6.7   Welded joint taken from [29].

7 FEM-based computation

This chapter presents the FEM, finite element method, used for solving the optimization problem against buckling and yielding in the study. Section 7.1 covers the mathematical method behind the global stiffness matrix, which is applied in many structure problems based on the beam theory. In Section 7.2, the procedure to obtain a global stress analysis matrix of the entire construction is described.

7.1 3D-Beam method

The geometrical change in the shape of the derrick and the variations of the strength property through the whole structure makes it impossible to use an analytical method to determine any reliable result of the stresses and the safety margin against failure in the critical zones of the structure.

The analysis of the entire derrick was simplified as a cantilever beam with the assumption of a constrained deformation at the bottom surface of the structure at the driller floor, see Figure 7.1
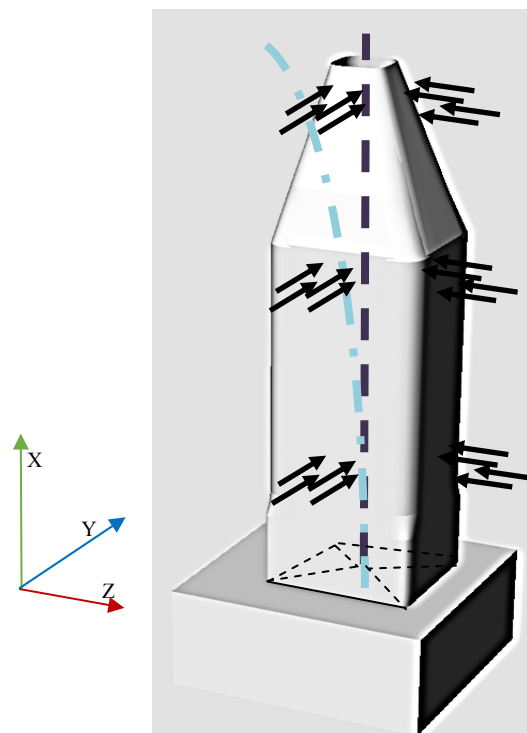
Figure 7.1   *Stress-deformation analysis of a stressed skin derrick utilizes the beam theory with deflection. The arrows represent the wind force acting on the derrick.*

A numerical approach, based on FEM established the values for defined nodes at the end of each vertical segment of the derrick structure. Each segment was defined as a horizontal section of the derrick, which was bounded by two transversal girders at its top and bottom. These were assigned by its specific geometrical properties such as the cross section area A, moment of inertia I_y and I_z and structural mass M.

The number of segments was directly dependent on the number of transversal stringers. Since the safety of the structure against buckling and yielding of the plate, stiffeners and stringers were checked with STIPLA [7] and [8], there was no need for more than one representative force vector for each segment. This vector contains 3 deflections in 3 global directions and 3 rotations around 3 global axes.

Furthermore, another assumption made in the study was that the centres of gravity of the drilling equipment pass through the shear centre of the transversal cross sections of the derrick, which means that the axial forces did not contribute to any torsional buckling. The lateral forces acting on the derrick, such as wind forces and accelerations from the rig, are also uniformly distributed in each horizontal level and their resultant was assumed to pass through the shear centre of the cross section.

These two load conditions acting on the derrick resulted in a case of pure bending and shear forces due to the fact that twisting was eliminated in the current study.

In order to precisely determine property changes related to the strength and the elasticity in the transverse deformations and bending moment curves, a cantilever beam was modelled. This beam was divided into a set of beam elements. As mentioned earlier, the number of these elements depended on the chosen spacing between the transversal stringers in the vertical direction, namely segments. Each element had two nodes at its ends and each node generated 6 degrees of freedom, 3 in a length deformation in each direction and 3 in a rotational deformation around each defined moment axis. A fixed boundary condition at the bottom of the derrick set these degrees of freedom to zero.

These elements built up a set-up of number of "springs" connected to each other and the final deformation was determined by the simple force-displacement relations of a string by a weak formulation that used the principle of minimum of the potential energy according to Paz and Leigh [6], equation (7.1)

$$F = Kw \Rightarrow w = K^{-1}F \qquad\qquad (7.1)$$

where,

$F =$ force
$K =$ spring stiffness
$w =$ displacement

7.2 Global stiffness matrix

A local stiffness matrix for a three-dimensional beam element was set for each beam element according to Paz and Leigh [6], see Figure 7.2. Each beam element represented two nodes at the top and at the bottom. The length of these elements were free to vary in calculations, but not allowed to exceed the vertical distances between each two transversal stringers, namely segments.

$$
\begin{bmatrix}
\frac{EA}{L} & & & & & & & & & & & \\
0 & \frac{12EI_z}{L^3} & & & & & & \text{Symmetric} & & & & \\
0 & 0 & \frac{12EI_y}{L^3} & & & & & & & & & \\
0 & 0 & 0 & \frac{GI}{L} & & & & & & & & \\
0 & 0 & \frac{-6EI_y}{L^2} & 0 & \frac{4EI_y}{L} & & & & & & & \\
0 & \frac{6EI_z}{L^2} & 0 & 0 & 0 & \frac{4EI_y}{L} & & & & & & \\
0 & 0 & 0 & 0 & 0 & 0 & \frac{EA}{L} & & & & & \\
\frac{-EA}{L} & \frac{-12EI_z}{L^3} & 0 & 0 & 0 & \frac{-6EI_z}{L^2} & 0 & \frac{12EI_z}{L^3} & & & & \\
0 & 0 & \frac{-12EI_y}{L^3} & 0 & \frac{6EI_y}{L^2} & 0 & 0 & 0 & \frac{12EI_y}{L^3} & & & \\
0 & 0 & 0 & \frac{-GI}{L} & 0 & 0 & 0 & 0 & 0 & \frac{GI}{L} & & \\
0 & 0 & \frac{-6EI_y}{L^2} & 0 & \frac{2EI_y}{L} & 0 & 0 & 0 & \frac{6EI_y}{L^2} & 0 & \frac{4EI_y}{L} & \\
0 & \frac{6EI_z}{L^2} & 0 & 0 & 0 & \frac{2EI_z}{L} & 0 & \frac{-6EI_z}{L^2} & 0 & 0 & 0 & \frac{4EI_z}{L}
\end{bmatrix}
$$

Figure 7.2   Local stiffness matrix, 12x12 elements.

A global matrix of the entire beam was assembled using all local stiffness matrices as in Equation (7.2)

$$
K_{Global} = \sum_{i=1}^{elements} k_{local_i} \tag{7.2}
$$

The force applied for calculating the deflections of all free nodes was located as point forces on each free node and possible hydro forces were located as pressure along the beam. Both static and dynamic forces were calculated according to the shear force difference between each node in the corresponding direction from the global model. These remained constant independently of the dimensions of the horizontal cross section.

The absorbing internal shear forces and bending moments of the structure were calculated based on the considered deflections and rotations at each node, respectively, according to Paz and Leigh [6]. Both the deflection vector and force vector were calculated according to Equations (7.3)-(7.8) and contained 6 elements for each node see Figure 7.3.

$$
F_x(i) = -\frac{AE}{L}(w_{i_x} - w_{(i+1)_x}) \tag{7.3}
$$

$$F_y(i) = -EI_z\left[\frac{12}{L^3}, \frac{6}{L^2}, \frac{-12}{L^3}, \frac{6}{L^2}\right] \cdot \left[w_{i_y}, \theta_{i_z}, w_{(i+1)y}, \theta_{(i+1)z}\right]$$

(7.4)

$$F_z(i) = -EI_y\left[\frac{12}{L^3}, \frac{-6}{L^2}, \frac{-12}{L^3}, \frac{-6}{L^2}\right] \cdot \left[w_{i_z}, \theta_{i_y}, w_{(i+1)z}, \theta_{(i+1)y}\right]$$

(7.5)

$$M_x(i) = -\frac{GI}{L}(\theta_{i_x} - \theta_{(i+1)_x})$$

(7.6)

$$M_y(i) = -EI_y\left[\frac{12x}{L^3} - \frac{6}{L^2}, \frac{4}{L} - \frac{6x}{L^2}, \frac{-12x}{L^3} + \frac{6}{L^2}, \frac{-6x}{L^2} + \frac{2}{L}\right] \cdot \left[w_{i_z}, \theta_{i_y}, w_{(i+1)z}, \theta_{(i+1)y}\right]$$

(7.7)

$$M_z(i) = -EI_z\left[\frac{12x}{L^3} + \frac{6}{L^2}, \frac{4}{L} - \frac{6x}{L^2}, \frac{-12x}{L^3} - \frac{6}{L^2}, \frac{-6x}{L^2} + \frac{2}{L}\right] \cdot \left[w_{i_y}, \theta_{i_z}, w_{(i+1)y}, \theta_{(i+1)z}\right]$$

(7.8)

7.3 Global stresses

The calculations of the global stresses were based on the deflections of the horizontal cross sections along the beam structure. The main stress magnitude required for a buckling/ yielding analysis was based on the following:

- Axial forces acting on the stiffened plate
- Shear stress
- Transversal stresses acting on the stiffened plate
- von Mises (equivalent effective) stress

Furthermore, the local lateral pressure acting on the stiffeners/ stringers also needed to be considered. The lateral pressure appears as either wind pressure and/or transversal pressure from setback, see Figure 7.3
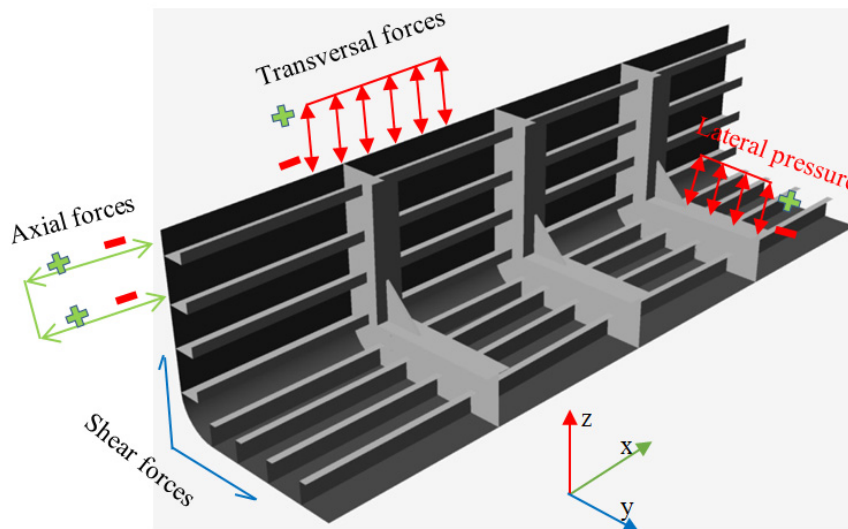
Figure 7.3   Visualization of the stresses for analysis of buckling and yielding.

The axial stresses in each beam were calculated from axial forces due to the weight of the structural steel and equipment. The biaxial bending moment of the derrick will contribute to the axial stresses according to Equation (7.9) for a beam structure according to Ringsberg [24].

$$\sigma_X = \frac{N}{A} + \frac{(M_Y I_{YZ} + M_Z I_Y) \cdot Y - (M_Z I_{YZ} + M_Y I_Z) \cdot Z}{I_{YZ}^2 - I_Y I_Z} \tag{7.9}$$

where,

σ_x = axial stress,
N = axial force,
A = cross section area
M_Y, M_z = bending moment in the respective direction
I_Y, I_z = moment of inertia in the respective cross section
I_{YZ} = product of inertia

Shear stress calculation was based on a closed thin-walled cross section type from Equation (7.4) according to te Canadian Institute of Steel Construction [30].

$$\tau_{max} = \frac{V}{C_{RT}}, \text{ where } C_{RT} \approx 2t(h - 4t) \tag{7.10}$$

In Equation (7.10),

τ = shear stress,
C_{RT} = Torsional constant for a hollow section with a rounded corner,
V = shear forces,

Since in the present study the aim was not to consider the effect of local stresses, it was recommended that further calculation was free to be based on the magnitude of transversal stresses based on a previous master's thesis written by Johansson [12], see Appendix B for the stress plot.

The von Mises stresses were calculated for an assumption of the plane stress condition as in Equation (5.4) in Section 5.3

8 Optimization

In the present sections, an introduction of the general optimization theory is presented as well as an available optimization method for minimizing the weight of a derrick against yielding and buckling. In Section 8.1 a basic general optimization theory and a different method are described. In Section 8.2, a presentation of the chosen optimization method in the present study is described. In Section 8.3 the methodology of weight optimization of a derrick is discussed extensively.

8.1 General optimization theory

There are many techniques available for the solution of a constrained nonlinear programming problem. All the methods can be classified into two broad categories: direct methods and indirect methods, as shown in Figure 8.1. In the *direct methods*, the constraints are handled in an explicit manner, whereas in most of the *indirect methods*, the constrained problem is solved as a sequence of unconstrained minimization problems. The idea is to find the best optimization solution for the problem.
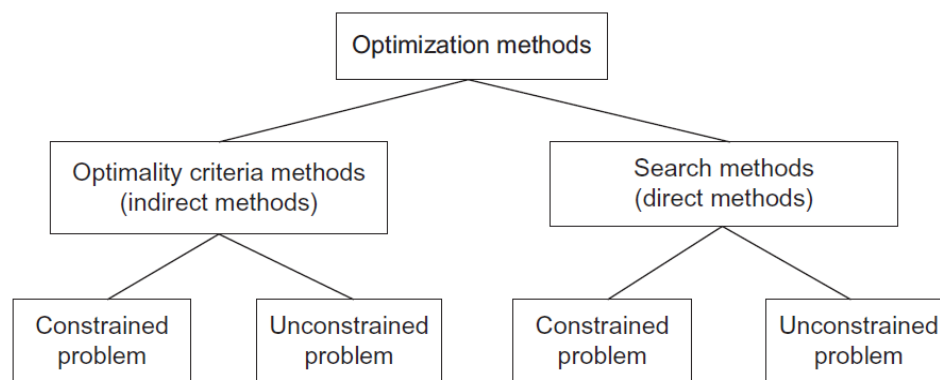
Figure 8.1   Non-linear optimization methods.

8.2 Nonlinear Constrained optimization

Nonlinear constrained optimization is an optimization method that minimizes a function $f(x)$, called the objective function. The idea is to find a vector x called the design variables, which is a local minimum to a scalar function $f(x)$ subjected to some constraint. The constraints are the function that needs to be fulfilled during the optimization. The constraints can be either equality or inequality and also linear or nonlinear. The variable x can be either one variable or a vector with multiple variables. This function can be written as the following:

Find x which minimizes $f(x)$ *(objective function)*   (8.1)

Subject to

$g_j(x) \leq 0, j = 1, 2,..., m$ *(Inequality constraint)*   (8.2)

$h_k(x) = 0, k = 1, 2,..., p$ *(Equality constraint)*   (8.3)

The variable/variables x can also be constrained with a lower and upper boundary to make the optimization search for finding the minimum $f(x)$ faster. The optimization is clearly utilized in Figure 8.2 with a simple mathematical function taken from [31]. Most of the optimization methods use the gradient-based method in order to minimize or maximize the objective function. The mathematical expression in Figure 8.2 can be written as follows:

$$\text{Find } x, \text{ which minimizes } f(x) = x_1 + 2x_2 \tag{8.3}$$

Subject with constraints

$$3x_1 + 2x_2 \geq 6, \qquad 2x_1 + 3x_2 \leq 12, \tag{8.4}$$

With an upper and lower boundary

$$0 \leq x_1, \, x_2 \leq 5, \tag{8.5}$$
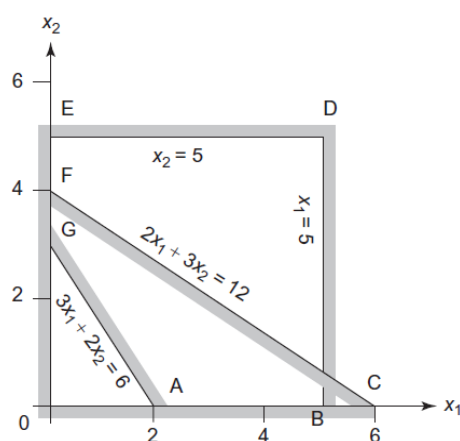
Figure 8.2   Visualized optimization problem, from [31].

In the Matlab Optimization Toolbox [5] the *fmincon* routine solves constraint problems. The *fmincon* routine in Matlab has four algorithms for solving the problems, which are the following according to the *Matlab* help function:

- The interior point algorithm is used for general nonlinear optimization. It is especially useful for large-scale problems that have sparsity or structure, and tolerates user-defined objective and constraint-function evaluation failures. It is based on a barrier function, and optionally keeps all iterates strictly feasible with respect to bounds during the optimization run.

- The SQP algorithm is used for general nonlinear optimization. It honors bounds at all iterations and tolerates user-defined objective and constraint function evaluation failures.

- The active-set algorithm is used for general nonlinear optimization.

- The trust-region reflective algorithm is used for bound constraint problems or linear equalities only. It is especially useful for large-scale problems.

If the algorithm is not specified by the user, *fmincon* automatically chooses the algorithm which suits the problem objective function and constraints.

8.3 Optimization methodology

In Figure 8.3, the methodology of the optimization is shown. Optimization of the derrick was based on the optimization of the total structure weight against yielding- and buckling capacity due to the most critical load cases during the operation. As mentioned in the description of the project, it was not aimed at making any extensive geometry changes of the outer shell of the derrick.
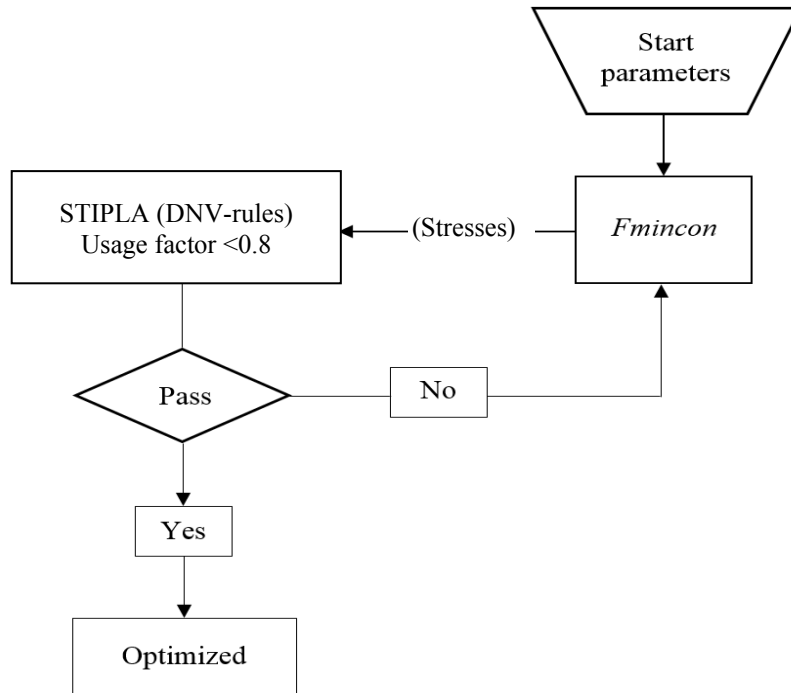
Figure 8.3   Schematic optimization methodology.

In Figure 8.3, the start parameters influent on the structure weight are defined as a matrix containing; the spacing between stiffeners, thickness of plates around the cross section, cross section profile dimensions of longitudinal stiffeners and profile dimensions of the transversal stringers, see also Figure 8.4. These initial parameters, together with the loads, give a matrix of stresses along the entire derrick structure as output. These stresses, together with the current design according to the initial parameters, result in different usage factor according to DNV rules [9], [10] and [11]. The usage factors as described in Tables 5.4 and 5.5, need to be checked against the permissible usage factor according to the design criteria. If these rechecked usage factors are within the frame of the constraints span, the last input variables will be maintained as a final optimized result. If not, the procedure has to be continued till the set of parameters results in the smallest structural weight meaning that the optimized parameters are reached and obviously still constrained by DNV standard rules.

The weight optimization used the numerical script in Matlab by defining the total mass of stressed skin as an objective function in *fmincon*. The calculation was based on varying and finding the value of the multipliers, in this case the parameters in each cross sections, which made the basis of the strength of the structure such that the output structure weight was the minimum of this objective function. The constraints of the optimization for variable parameters were defined as maximum usage factors in

Tables 5.4 and 5.5. The presented usage factor in Tables 5.4 and 5.5 are a result of different dimensioning against defined axial/transversal stresses in the stiffened plate field.

The variable parameters in each horizontal cross section were as follows:

- Profile parameters of the longitudinal L-stiffeners
- Profile parameters of the transversal T-stringers
- Plate thickness of the outer shell of the derrick
- Spacing between the longitudinal L-stiffeners around the circuit of the derrick structure's inner plate field, see Figure 8.4.
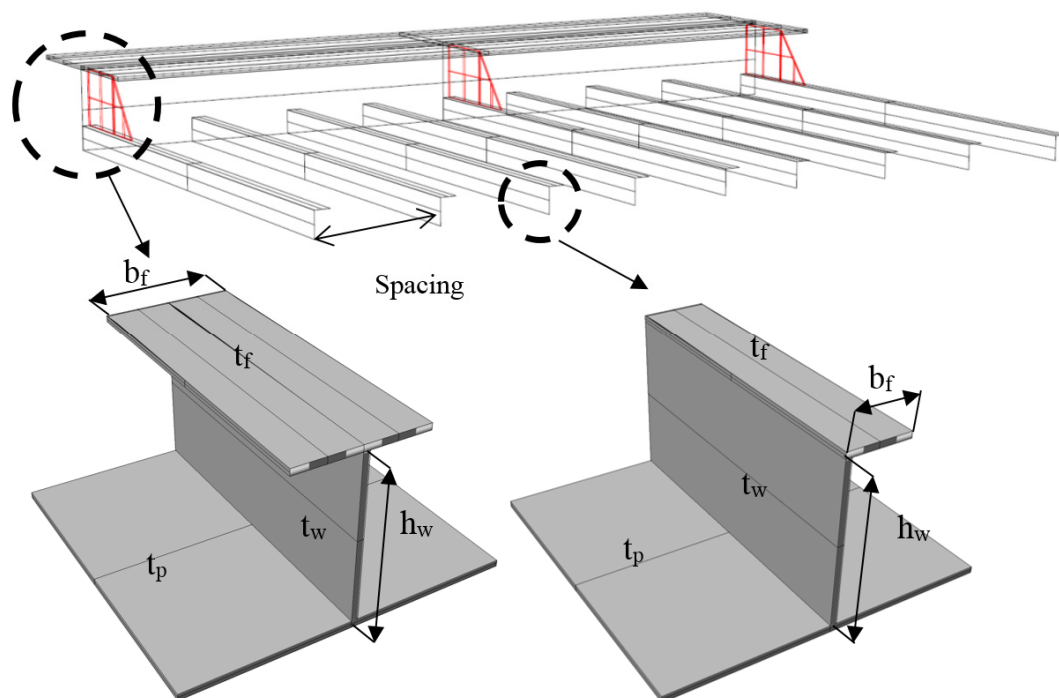
Figure 8.4   Variable parameters during the optimization process.

Since the entire construction was considered as a cantilever beam with fixed supports at the driller floor, the critical stresses against buckling and yielding occurred in the lower levels of the derrick. This means that dividing the height of the structure and assigning the optimization parameters of each segment its exclusive values, ends with results closer to the final optimum.

The outer plate thickness of the derrick structure has a major influence on both the strength and weight of the derrick. Finding the optimum plate thickness is an important parameter in the study. About 60-70% of the forces are carried by the thickness of the plate.

Spacing of the stiffeners and stringers is another influential parameter of strength and the mass of derrick. By choosing the optimum spacing between the longitudinal stiffeners and transverse stringer in order to sustain the stresses in the derrick, the number of stiffeners and stringers can be kept at the minimum index.

The number of segments depended on the number of the transversal stringers.

Stringers in the derrick act more as a support of the longitudinal stiffeners and resist the buckling of these rather than acting as a resistant web due to the torsional stresses between the opposite sides of the outer shell. This was the reason why scantling of the spacing between the transversal stringers was determined before the optimization started. The vertical distance between these stringers was based on the highest carrying capacity and the lowest risk of buckling of the vertically running stiffeners.

The numerical calculations of the strength of the structure steel required a Matlab routine containing:

- Geometry of the draft design
- Data for the proposed material
- Calculation of the force (operational and structural)
- Calculation of the deformations and stresses, by an FE-method based on stiffness matrix

Furthermore, the optimizer routine based on *fmincon* required an objective function, in this case the final total structural mass, and also a routine containing the constraints of the optimization. See Tables 5.4 and 5.5 for all usage factors used as constraints in *fmincon*.

The usage factors in this case were calculated by the STIPLA [7] and [8]. After each parameter changes, the call of STIPLA-file was implemented via Matlab. Afterwards, the output text file formed the basis of further iterations for lower/higher assigned parameter values, see Figure 8.5.
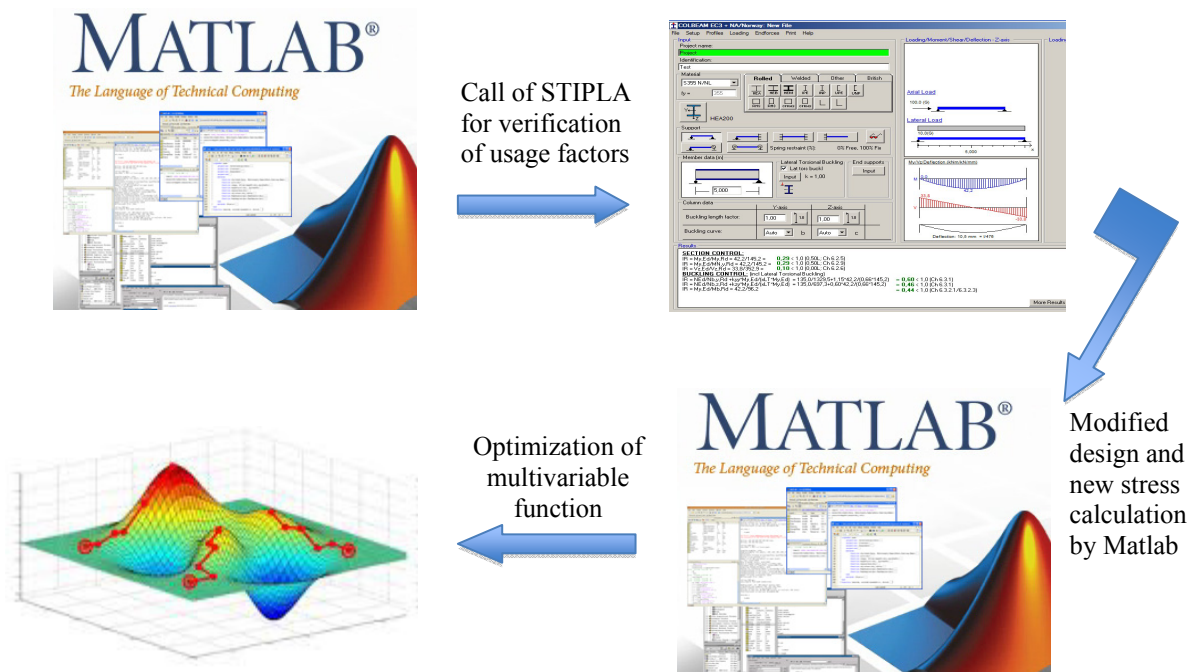
Figure 8.5   The procedure of optimization of the multivariable function.

Studying the development of optimization using *fmincon,* indicated the fact that the keyword here was the choice of the initial values, which, fallen to calculations of the multipliers, had to be restricted within the framework of constraints. It was for feasibility reasons that the gradient of the objective function looked for the minimum function value depending on the development of the derivation of the function. In any case, if the search failed at the start iteration, *fmincon* would not continue the optimization and responded with an error in the calculations.

Since the entire derrick structure was considered as a cantilever beam, the optimization had to start at the highest top section and the optimized values of each specific section needed in order to be saved for further operations for all segments below this for the lowest possible structural mass, see Figure 8.6.
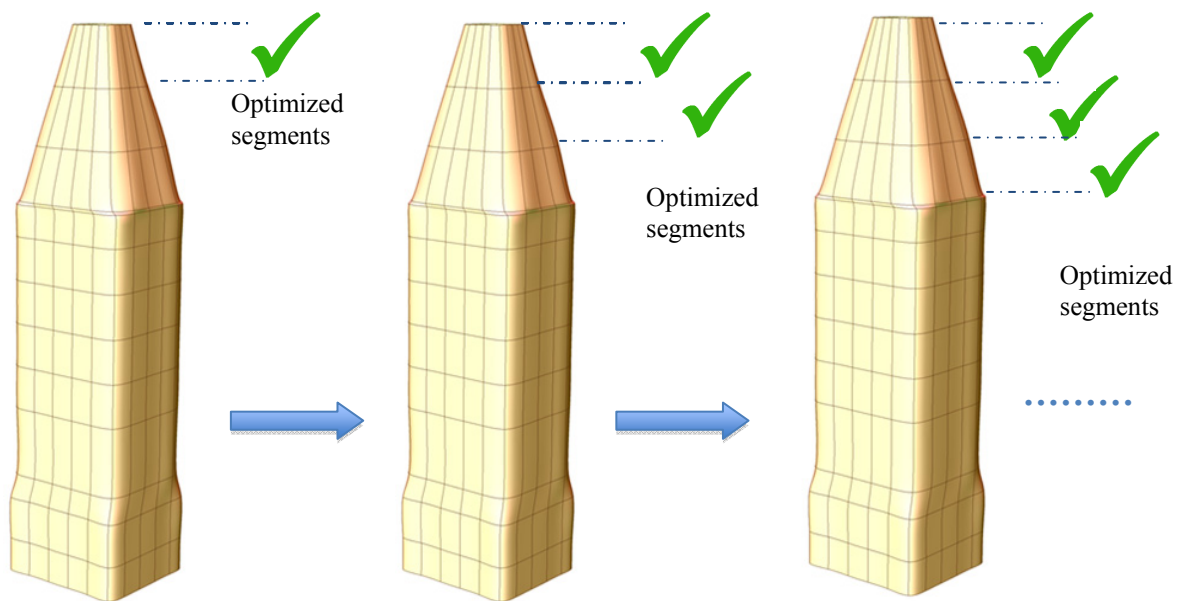
Figure 8.6   *The optimization restricts variable parameters to only the current ones at each segment in order not to involve too many variables at the same time. This keeps the optimization time at its lowest possible.*

9 Results and discussion

In this chapter, the results after each weight optimization against yielding and buckling are presented with an initial starting point for the optimization. Results and the final weight of the derrick with all dimensions are represented in Section 9.1. In Section 9.2, results of forces and moments are presented for the final iteration. The deformation and stresses of the derrick is utilized and described in Section 9.3. In Section 9.4, a comparison of costs was made compared to the covered truss derrick and in Section 9.5, a discussion about optimized results is made.

9.1 Results of weight optimization

The results in Tables 9.2 and Appendix B are the structural elements dimension for each segment between the stringers after optimization iteration. In each iteration, the spacing of stiffeners was changed in order to find the optimum derrick weight. The initial parameters for the final iteration are presented in Table 9.1. The structural weight with the initial parameter was calculated to 590 mT.

Table 9.1   Initial parameter for the final optimization iteration.

Seg.	Segm. height [m]	Plate Head/Beam [mm]	Stiffener dimension[mm]	Stringer dimension[mm]	Spacing stiffener head [mm]	Spacing stiffener beam [mm]
1	6.6	10	130x80x13x13	150x90x12x12	600	600
2	6.6	10	140x90x13x13	210x100x15x15	600	600
3	6.6	13	150x90x16x16	250x170x16x16	600	600
4	4.95	13	150x90x16x16	380x180x22x22	600	600
5	4.95	15	150x90x16x16	420x180x22x22	600	600
6	4.95	15	150x90x16x16	440x180x22x22	600	600
7	4.95	15	160x90x16x16	470x180x23x23	600	600
8	4.95	15	160x90x17x17	490x180x24x24	600	600
9	4.95	15	170x90x18x18	530x180x24x24	600	600
10	4.95	15	180x90x18x18	550x180x24x24	600	600
11	4.5	20	180x90x18x18	650x200x26x26	600	600
12	4.5	20	180x90x18x18	750x230x26x26	600	600

The results from the final optimization are presented in Table 9.2. The results from optimization were a rounded integer. The thicknesses were rounded with 1 mm and flanges and webs with 10 mm. The rounding is a consideration to the manufacturing and shipyard standard manufacturing dimension. The obtained weight for a stressed skin derrick in the final iteration was 424 mT with a reduction in the vertical centre of gravity of 1.5 m. The most reduction of the structural weight compared to the previous master's thesis study by Johansson [12] was due to the number of the transversal stringers. Especially in the highest part of the derrick, the lesser number of supporting transversal stringers means huge difference in the stress magnitude due to the bending moment of the total structure. This occurs because of a lesser mass at locations with a larger moment arm at the top levels. A lesser bending moment definitely requires less reinforcement along the total structure and the total mass will be reduced significantly.

Table 9.2   Final result from optimization.

Seg.	Segm. height [m]	Plate, head [mm]	Plate beam [mm]	Stiffener dimensions [mm]	Stringer dimensions [mm]	Spacing stiffener head [mm]	Spacing stiffener beam [mm]
1	6.6	8	8	100x80x12x10	140x100x11x11	600	600
2	6.6	8	8	140x90x11x11	210x100x11x12	600	600
3	6.6	9	9	140x90x15x14	250x180x13x17	600	600
4	4.95	8	8	130x90x10x10	380x180x18x18	600	600
5	4.95	9	10	130x90x13x13	420x180x16x17	600	600
6	4.95	10	10	130x90x14x14	450x180x18x17	600	600
7	4.95	11	11	140x90x13x12	470x180x19x19	600	600
8	4.95	11	11	150x90x14x15	490x180x20x20	600	600
9	4.95	13	11	150x90x16x15	520x180x19x20	600	600
10	4.95	13	12	160x90x17x17	550x180x20x20	600	600
11	4.5	12	12	150x90x14x15	680x180x21x22	600	600
12	4.5	12	12	160x90x15x16	700x180x22x23	600	600

The total weight of the derrick with brackets and additional weight due to welding is shown in Table 9.3.

Table 9.3   Total weight of the derrick.

Contributory	Weights [mT]
Total structural derrick	424
Brackets	20
Welding	21
Sum	**465**

The parts in brackets include both tripping brackets between longitudinal and transversal stiffeners and also horizontal support brackets between horizontally orthogonal stringers, see Figure 6.4.

9.2 Results of moment and shear forces

In Figures 9.1-9.3 the shear force/moment diagrams for load case head, beam and quart are visualized. The diagrams in Figures 9.1-9.3 show the bending moment and the shear forces, respectively, along the derrick structure in all load cases in the current study.
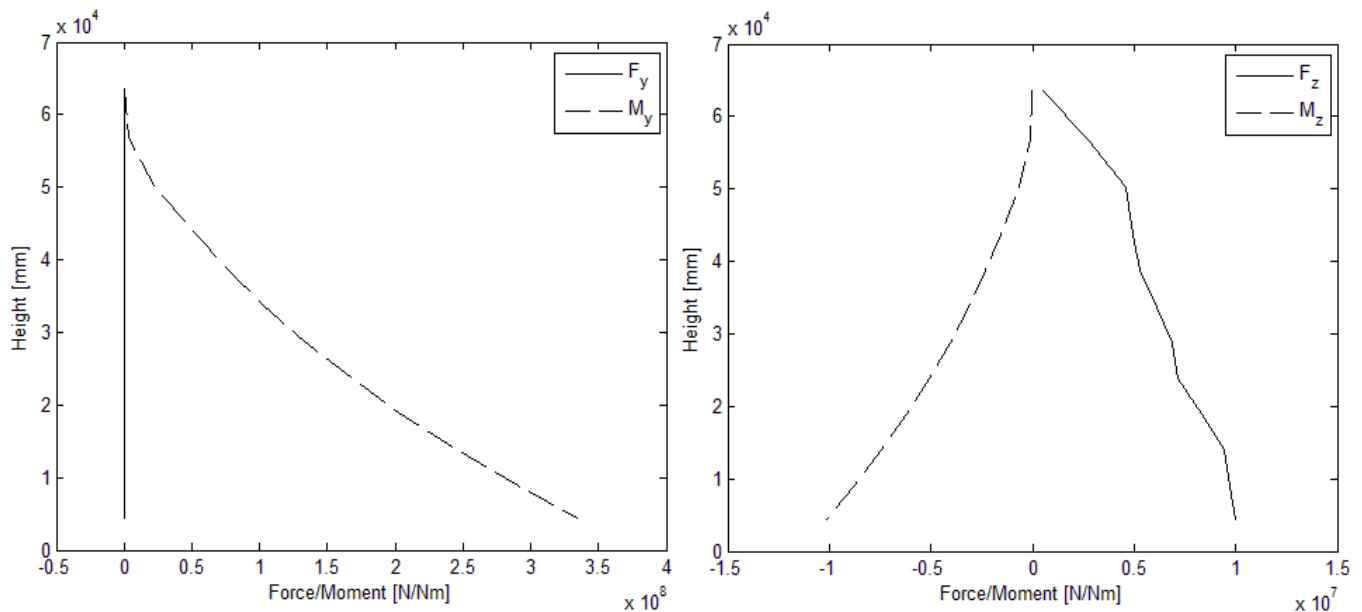
Figure 9.1   Shear force and bending moment diagram, head sea.

As was expected, the bending moments increased exponentially right down to the bottom since the transversal loads are unequally distributed along the height of the derrick. The magnitudes of the transversal shear forces were near zero.
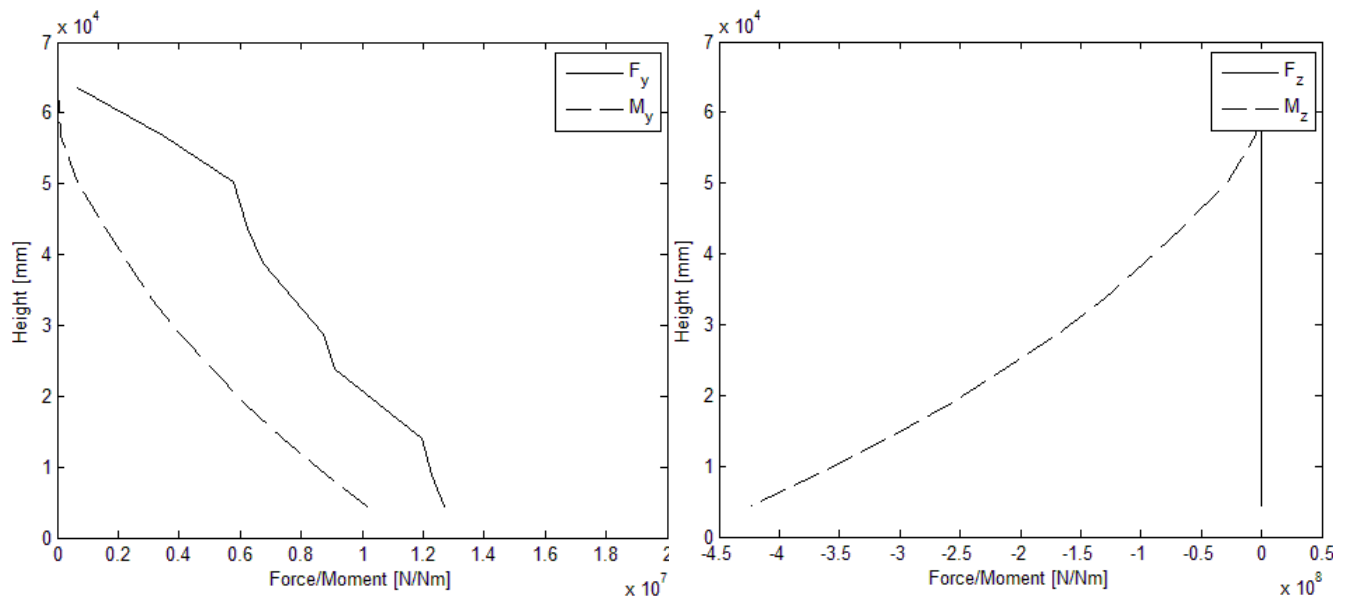
Figure 9.2   Shear force and moment diagram, beam sea.

The different shape in Figure 9.2 compared to the force and moment diagram in Figure 9.1 depends on the relatively low rig acceleration at beam sea for bending around the global y-axis. The vertical shape in Figure 9.2 is because of the near zero shear forces in the derrick at beam sea.
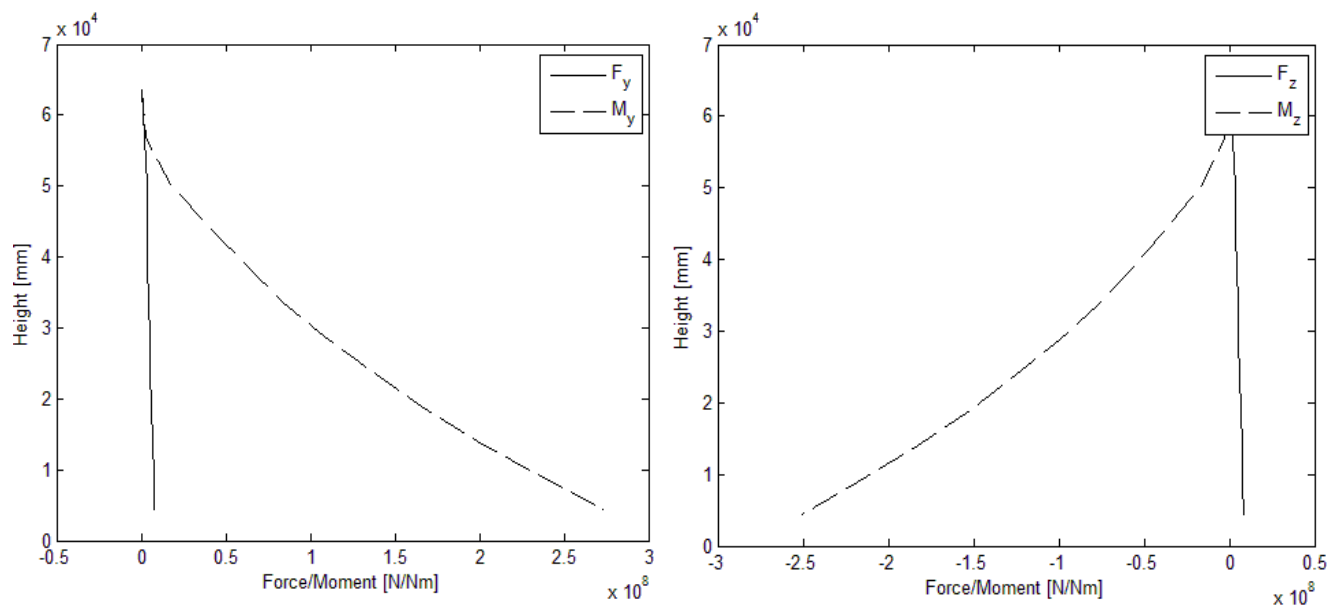
Figure 9.3   Shear force and moment diagram, quart sea.

Analyzing the forces and moments at quart sea, it was shown that the magnitude of the bending moment around the global y-axis, i.e. forward and aft, were larger than those for port and starboard. This was expected since the lengths of these sides are larger than port and starboard. However, the shear forces showed insignificant differences.

9.3 Results of deformations and stresses

The axial stresses of the derrick structure due to the bending were schematically shown in Figure 9.4. The most critical axial stresses were located at the outermost fibres in the forward, starboard, aft and port sides. This is because the moment arm is largest at these points.
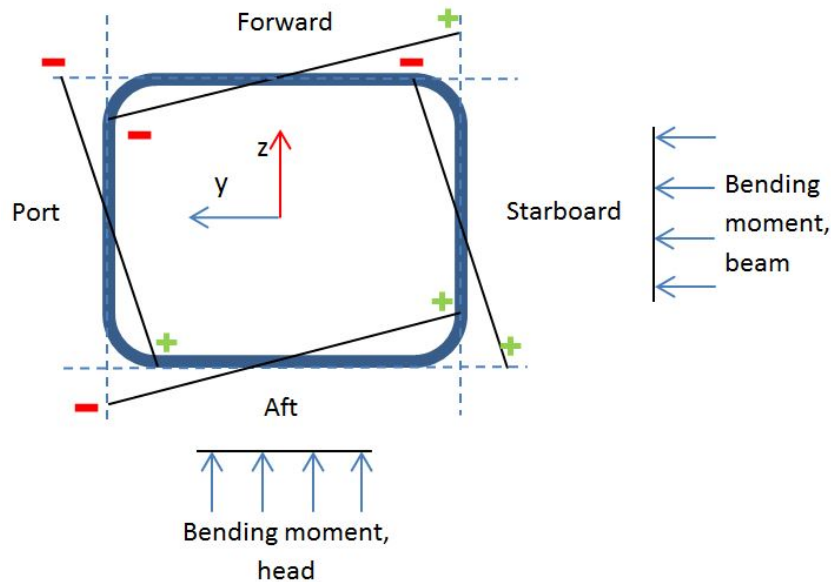
Figure 9.4   Axial stresses on the derrick's outer shell due to the bending moments.

The positive and negative signs in Figure 9.4 visualize compression and tension stresses, respectively.

Figure 9.5 presents global deformations of the entire derrick structure at the most critical load case, i.e. quart sea.
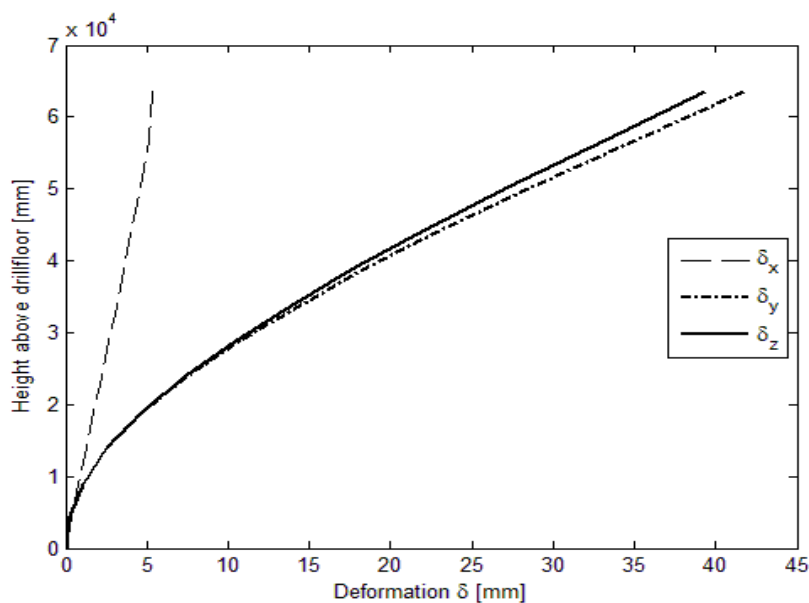
Figure 9.5   Deformation of derrick structure at quart sea.

Deformations of the derrick structure had the expected values for a cantilever beam structure with a fixed support at the bottom of drill floor. Development of the deflections of the derrick structure had rather a similar pattern in the respective directions in head and beam load cases.

Figure 9.6 presents compressive stresses of the two most critical zones along the derrick structure in all load cases of this study. Since the derrick structure as a cantilever beam deals with a biaxial bending moment case the most critical zones, as was expected, occurs at corners between different outer plates. The most critical zone locates at the edge between aft and starboard since the bending moments are definitely negative at these locations and result in the most compressive stresses.
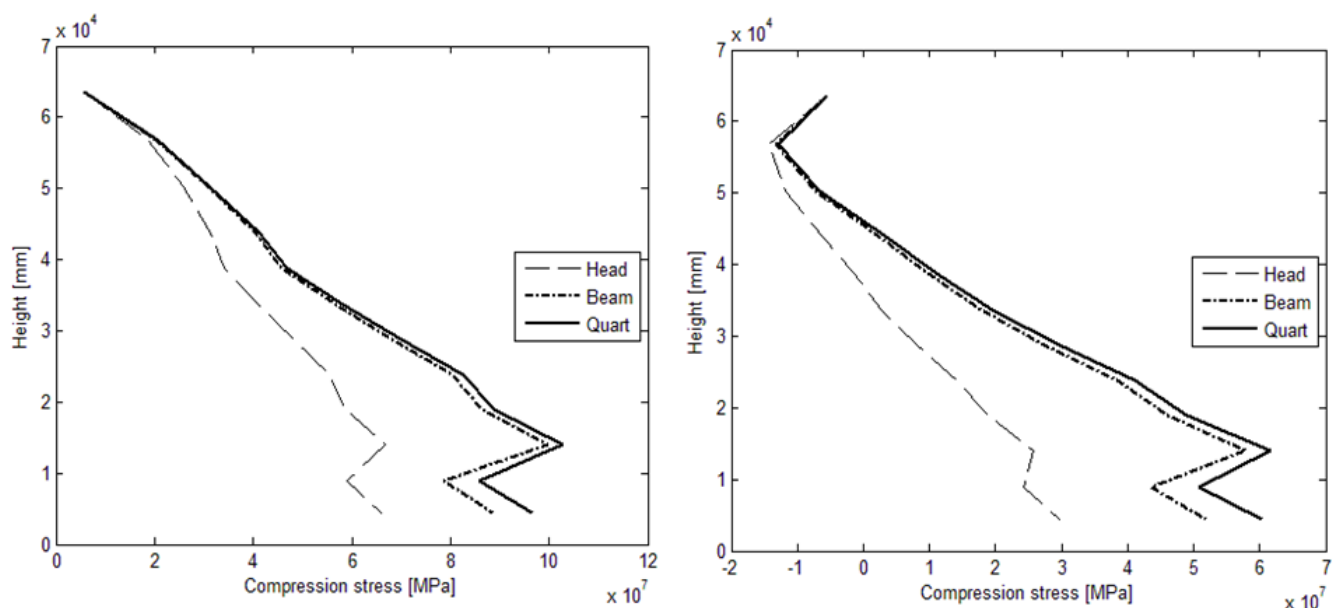
Figure 9.6   Compressive stresses. In the left, corner between port and forward. In the right, corner between starboard and forward.

In both cases in Figure 9.6, the height of one of the most critical zones locates at the top of the bottom section, where the outer shell starts to grow a 2 m radius in all corners. It was expected that the highest values should occur at the bottommost levels, but since the vertical reinforcement of the bottom section is higher than the mid-section, the stresses at the most bottom part of the mid-section also count as critical. This is because of the possibility of designing a greater number of vertical stiffeners due to the straight shape all the way to the corners at the bottom section. This makes the cross section at this level vertically stronger against compressive loads and the "notch" of all curves in Figure 9.6 at 13.5 m depends on this.

Table 9.4 contains von Mises-, shear-, and axial compressive stresses and the critical usage factors for each segment with notations which were explained above in Tables 5.4 and 5.5. All offered values in Table 9.4 are the most critical ones that optimization converged to constraints, namely the usage factor.

Table 9.4   Critical stresses and usage factor for final iteration.

Seg.	Seg. height [m]	von Mises stress, σ_{vM} [MPa]	Shear stress, τ_{xy} [MPa]	Shear stress, τ_{xz} [MPa]	Comp. stress, σ_x [MPa]	Critical usage factor	Usage factor value
1	6.6	15	8	6	-6	UF_s	0.74
2	6.6	47	23	18	-24	UF_s	0.78
3	6.6	59	25	20	-34	UF_g	0.8
4	4.95	65	21	17	-48	UF_g	0.8
5	4.95	80	23	18	-56	UF_g	0.8
6	4.95	95	26	21	-65	UF_s	0.79
7	4.95	109	29	23	-79	UF_p	0.78
8	4.95	122	29	23	-91	UF_g	0.78
9	4.95	138	34	27	-103	UF_g	0.8
10	4.95	150	38	30	-113	UF_g	0.8
11	4.5	120	31	25	-110	UF_g	0.8
12	4.5	128	30	24	-120	UF_s	0.8

Table 9.4 shows that the equivalent effective stress or von Mises are under permissible stresses, 284 MPa. This verifies the conclusion mentioned above in the report that buckling is the governing design criteria and yielding will not occur before buckling for the new derrick design. Furthermore, since the transversal forces are relatively small in all different load cases, the shear stresses are small also. The usage factors presented in Table 9.4 are only the most critical ones. From Table 9.4, it is observed that most critical buckling mode in the top section of the derrick, segments 1 and 2 is stiffener buckling. In the middle section and bottom of the structure, the buckling of the girder is the dominating effect.

9.4 Costs of a new design

The manufacturing costs for the achieved design are compared to the covered truss derrick estimated by Aker MH [3]. The manufacturing costs are presented in Table 9.5 for a covered truss derrick and this included material, labour and welding.

Table 9.5   Manufacturing costs for the reference truss derrick.

Contributory	Total weight [mT]	Price [NOK/kg]	Cost [MNOK]
Truss derrick	390	60	23.4
Enclose incl. beams	200	70	14
Total	590		37.4

The manufacturing costs of the stressed skin concept were based on a model for a typical stiffened shell construction with a variation in dimensions at different levels according to Farkas [32].

The modelling costs of the stressed skin derrick were according to Equation (9.1):

$$F_{total} = F_{mat} + F_{cons} + F_{lab} \qquad (9.1)$$

where,

F_{mat} = cost of materials

F_{cons} = cost of consumables

F_{lab} = cost of operators

Values of the total costs for the new stressed skin are presented in Table 9.6. The calculations of F_{mat}, F_{cons} and F_{lab} are presented in more detail in Appendix C. The value and derivation to the cost analysis is based on information given by Aker MH.

Table 9.6   Manufacturing costs for the reference derrick.

F_{mat} [MNOK]	7.82
F_{cons} [MNOK]	0.17
F_{lab} [MNOK]	26.12
F_{total} [MNOK]	33.21

Table 9.6 shows that the largest part of the manufacturing costs is due to the man-hour labour cost.

Figure 9.7 also shows the increase of the manufacturing cost of both the reference derrick and the new stressed skin concept. The manufacturing costs of the new stressed skin derrick showed a slightly steeper development against growing structural weight. This is due to the higher labour costs for a relatively more expected welded area of the new design compared to the reference truss derrick.
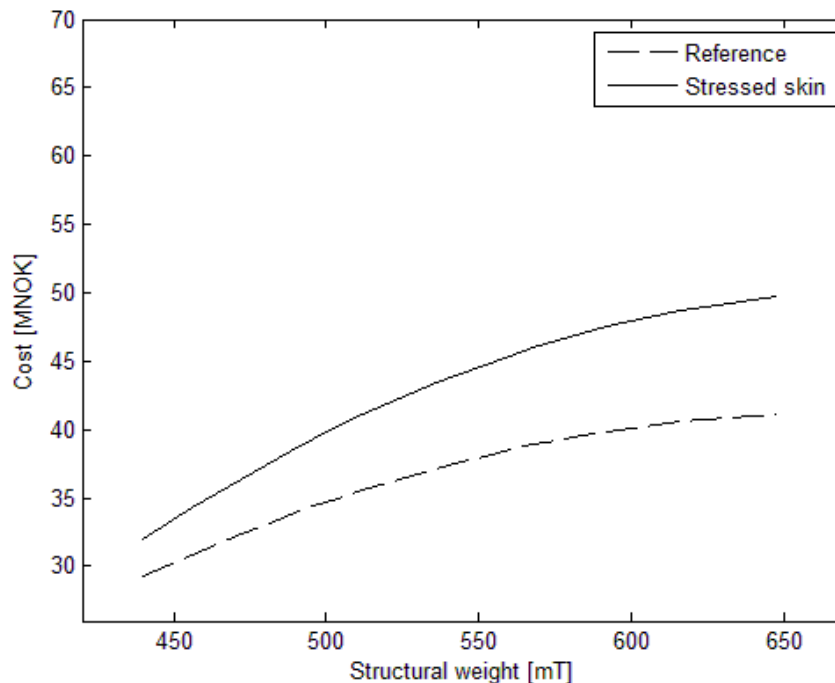
Figure 9.7   Manufacturing cost of reference derrick and stressed skin derrick.

9.5 Discussion

The final weight of the optimized derrick structure was calculated to 465 mT. The reduction in weight was 21% compared to an existing solution of a covered conventional truss derrick with a corrugated covering shell plate. The wind moment caused by the geometry of an enclosed stiffened shell was decreased by introducing rounded corners with a sufficient radius. This gave an indication of a future investigation of the enclosed solution..

Analyzing the method of numerical optimization using Matlab, it was established that this was a reliable method. When checking the "optimized" values for the respective objective function as the total structural mass of the derrick, it was found that these are chosen for an accuracy of 0.001 mm in order to get as close a gradient of zero as possible in the objective function development.

The results show that buckling is the governing failure mode of the structure. With this being said, one can conclude that the main part of the structure is governed by buckling and in order to optimize the structure, it is important to get the buckling criteria incorporated in the optimization algorithm. Considering a permissible usage factor as the design criteria it had been discovered earlier that further optimization against yielding would not have been necessary.

Because of the simple modeling, the equipment's contributions of the lateral loads to the stiffened shell were set to data from the FE-model in last year's master's thesis. Furthermore, it is assumed that local reinforcements in those regions are made.

Since the acting point of axial loads from the equipment's mass is set to the midpoint of each cross section, there were no torsional loads incorporated. For a more accurate design against torsional, even though this was not perceptible, it is recommended to add the moment of the applied torque by considering the more precise position of the mass centre of each equipment detail.

Studying a loaded stiffened plate from similar constructions, it was found that the plate carried 60-70 % of the axial loads and the longitudinal stiffeners supported the rest. This was a fact that influenced the optimization of the stiffeners by minor changes compared to the plate field.

When checking plate buckling it was noticed that the too small scantling of spacing between the transversal supporting stringers turns out to go against more critical usage factors. This was due to the large length of the stringers along the entire side of the outer shell. This caused a large self-weight which needed to be carried by the plate. Therefore it is highly recommended to investigate the option of separating the longitudinal stringers by two in order to reduce the tripping effect of these against the outer plate.

The presented values of optimized plate/stiffeners/stringers thicknesses in Section 9.1 were rounded to the closest integer. Further, the length/breadth of L-stiffeners and supportive T-stringers was rounded up or down to the nearest tenth.

Finally, an investigation of the economic financing in an enclosed derrick design showed a rather promising opportunity of investment in a new design. The cost of a stressed skin derrick was calculated to 33.21 MNOK, which is a reduction of almost 11%.

10 Conclusions

The possibility to design a covered conventional truss derrick as a stressed skin derrick has been investigated in the present study. The aim of the purposed design with a stressed skin derrick is to protect equipment against harsh weather conditions and to have the possibility to reach a lower structural weight compared to a covered conventional truss derrick. A reference derrick from Aker MH [3] has been used for obtaining the performance in aspects of strength, size and capacity, and converting it to an integrated steel panel construction instead

The weight of a covered conventional truss derrick used as a reference is 590 mT. The obtained structural weight of the stressed skin derrick in the present study is 465 mT with a 1.5 m reduction in VCG. The obtained weight is reasonable and in studies for a detailed design the weight may be amended with ± 20 tons with regard to the openings, which have not been taken into account in the present study

The following important conclusions are drawn from the performed study:

- Buckling is found to be the main governing failure criterion of the structure.

- Due to buckling being the governing failure criterion of the structure, a weight optimization against buckling strength is extremely important for obtaining an optimum structure dimension.

- In the study, only steel with a yield stress of 355 MPa was considered and an increase in yield stress would only give a small weight reduction, but, on the other hand, the manufacturing costs increase significantly.

- Introducing rounded corners in the derrick decrease the drag coefficient considerably, which leads to a lower wind moment and provides a preferable performance in stability condition.

- Due to a lower achieved weight and wind moment in the stressed skin derrick design, the solution provides a sustainable design with regard to less material and extraction of steel, but also a lower fuel consumption for positioning the drill unit in an upright condition for drilling operations.

- The stressed skin derrick manufacturing costs were reduced by 4.2MNOK compared to a covered conventional truss derrick.

- The optimization toolbox *fmincon* handled the optimization for reducing the stressed skin derrick weight in an optimum manner if the starting point for the optimization is inside the region of constraints.

11 Future work

In the current study several simplifications were made to be able to come up with an optimum stressed skin design of a derrick and investigate the possibility of reducing weight. Future work needs to be done in order to satisfy all design criteria specified by the classification society DNV in order to insure the safety of the design in all load conditions. The following future work is listed below:

- All loading conditions for every design condition in [9] must be analyzed and verified in order to ensure that sufficient structural strength is obtained. The worst loading condition must also be checked for every wave and wind direction.

- The drag coefficients in the present study were conservative. The drag coefficient for rounded corners with a higher Reynolds number needs to be investigated in order to obtain more specific values.

- The openings in the derrick need to be under study in a detailed design in order to specify the outer thickness, stringer and stiffener dimension in the bottom section of a derrick due to local effects. This will not influence the appreciable obtained weight.

- The equipment connections to the derrick and the position of equipment in the longitudinal and transverse directions need to be investigated in order to observe the local effects in the areas around the attachment of the equipment.

- Fatigue analyses shall be performed to investigate if changes are needed in structural elements.

- Lateral pressure from equipment due to acceleration of the rig needs to be verified in order to see if local dimension changes are needed.

- As was mentioned in the report, an FE-model analysis is necessary for the most critical fields as well as the effect of the notch factor in small details. For details with a more rounded shape and significant variations in geometry, an FE-model analysis is undoubtedly the easiest and fastest method.

12 References

[1] The Arctic Institute, http://www.thearcticinstitute.org/2013/04/arctic-oil-and-gas-hype-or-reality.html, [Cited 2013-04-16]

[2] USGS website, http://www.usgs.gov/newsroom/article.asp?ID=1980#.USsttlcUHzg, [Cited 2008-07-23]

[3] Aker MH, Derrick & Drillfloor Structural design brief, 170079-N-BA021-CA02-0101

[4] MathWorks, *MATLAB,* Version R2011a, Mars 18, 2011

[5] Coleman, Thomas, Branch, Mary Ann, Grace, Andrew (2007), *Optimization Toolbox 3,* Math works Inc.

[6] Paz, Mario, Leigh, William (2003): *Structural dynamics theory and computation*, Springer, US, Ch.13, pp.409

[7] StruProg AB, Structural Programs, *Stipla* DNVRPG, Version 2.0, April 2012

[8] StruProg AB, Structural Programs, *Stipla* DNVRPS, Version 2.1, Maj 2012

[9] DNV [Det Norske Veritas]. Offshore standard, structural design of offshore units (WSD method), Report DNV-OS-C201, April 2011

[10] DNV [Det Norske Veritas]. Offshore standard, Design of offshore steel structure general (LRFD method), Report DNV-OS-C101, April 2011

[11] DNV [Det Norske Veritas]. Recommended practice, buckling strength of plated structures, Report DNV-RP-C201, October 2010

[12] Johansson, Jens. (2012): *Development of a closed stressed skin derrick.* Chalmers University of technology, X-12/276, Gothenburg, Sweden

[13] DNV [Det Norske Veritas]. Recommended practice, environmental conditions and environmental loads, Report DNV-RP-C205, October 2010

[14] Autoship systems Corporation, *Autohydro,* 6.3.1, 2009

[15] Biran, Adrian (2003): *Ship hydrostatics and stability*, Oxford Butterworth-Heinemann, Jordan Hill, GBR, Ch.2, pp.39

[16] Gudmested, Ove T., Moe, Geir, *Hydrodynamic coefficient for calculation of hydrodynamic loads on offshore truss structures*, Marine structures, Vol.9, No.8, 09/1996, pp. 745-758

[17] Richter, Andreas, *Wind forces on square sections with various corner radii*, Hydromechanics university of Karlsruhe, 1984

[18]   Zheng, Chao-rong, Zhang, Yao-chun, *Numerical investigation on the drag reduction properties of a suction controlled high-rise building*, Journal of Zhejiang University SCIENCE A, Vol.11, No.7, 07/2010, pp. 477-487.

[19]   Zhou, Yongsheng, Q.S., Li, Shengli, Xu, *Numerical evaluation of wind effects on a tall steel building by CFD*, Journal of constructional steel research, Vol. 63, No. 5, 2007, pp. 612-627.

[20]   Holmes, John D. (2001): *Wind loading of structures*. Spon press, Mentone, Australia, Ch.4, pp.17

[21]   Newblod, Paul, Carlson, William L., Thorne, Betty. (2009): *Statistics for Business and Economics,* Pearson education, Ch.11, pp.463

[22]   Bulleit, William M. (2008), *Uncertainty in Structural Engineering,* Practice periodical on structural design and construction, ASE

[23]   Stamatelos, D.G; Labeas, G.N; Tserpes, K.I, *Analytical calculation of local buckling and post-buckling behaviour of isotropic and orthotropic stiffened panels, thin-walled structures,* Vol.49, No. 3, 2011, pp.422-430.

[24]   Ringsberg, Jonas (2011): *Marine structural engineering*. Department of shipping and marine technology, Gothenburg, Sweden

[25]   StruProg AB, *Theory Manual & Verification Documentation*, DNVRPS Version 2.1, Maj 2012

[26]   StruProg AB, *Theory Manual & Verification Documentation*, DNVRPG Version 2.0, April 2012

[27]   NURBS modeling for Windows, *Rhinoceros,* Version 4 SR9, Mars 9, 2011

[28]   Badran, Sherif Farouk, Saddek, Amr Bakr, Leheta, Heba Wael, *Ultimate strength of Y and T stiffeners subjected to lateral loads with three different levels of initial imperfection*, Ocean Engineering, Vol.61, 03/2013, pp.12.

[29]   Okumoto, Yasuhisa, Tekeda, Yu, Mano, Masaki, Okada, Tetsuo (2008): *Design of ship hull structures*, Springer, Verlag Berlin Heidelberg, Germany, Ch.9, pp.305

[30]   TORSIONAL SECTION PROPERTIES OF STEEL SHAPES (2002), Canadian Institute of Steel Construction

[31]   Arora, Jasbir (2011): *Introduction to optimum design*. Elservier, Australia, Ch.3, pp.80

[32]   Farkas, J. (2009), *Minimum cost design of a welded stiffened steel sectorial plate*, Steel Construction, Vol.2, 06/2009

Appendix A: Iteration results

In Appendix A, the results for different optimization results with a total structure mass, without brackets and welding weight are presented.

Table A.1   first Iteration result with all structure dimensions.

Seg.	Seg. length [m]	Plate Head [mm]	Plate Beam [mm]	Stiffener dimensions [mm]	Stringer dimensions [mm]	Spacing stiffener Head [mm]	Spacing stiffener Beam [mm]
1	6.6	7.5	7.5	104.4x75.0x12.2x12	119.3x89.3x11x11	650	600
2	6.6	8.5	8.5	133.3x85.5x13.3x13	229.1x99.1x14x14	650	600
3	6.6	9.5	9.5	142.5x85.5x15.2x15	263.7x168.7x16x16	650	600
4	4.95	9.3	9.3	139.8x83.9x14.9x15	385.5x175.5x20x20	650	600
5	4.95	10.8	10.8	135.0x81.0x14.4x14	425.7x175.7x20x20	650	600
6	4.95	11.3	11.3	140.7x84.4x15.0x15	446.6x176.6x21x21	650	600
7	4.95	11.2	11.2	149.6x84.1x15.0x15	475.6x175.7x22x22	650	600
8	4.95	11.5	11.5	153.3x86.3x16.3x16	506.8x176.9x23x23	650	600
9	4.95	12.4	12.4	161.5x85.5x17x17	537.7x177.7x23x23	650	600
10	4.95	12.5	12.5	173.5x86.8x17x17	567.8x177.8x23x23	650	600
11	4.5	14.0	14.0	168.4x84.2x16.8x17	654.4x194.1x24x24	650	600
12	4.5	13.9	13.9	166.3x83.1x16.6x17	691.8x192.5x24x24	650	600

The final structural weight for this iteration was calculated to 454mT. The weight with brackets and an additional welding weight was 495 mT.

Table A.2   Second Iteration results with all structure dimensions.

Seg.	Seg. length [m]	Plate, Head [mm]	Plate Beam [mm]	Stiffener dimensions [mm]	Stringer dimensions [mm]	Spacing stiffener Head [mm]	Spacing stiffener Beam [mm]
1	6.6	7,5	7,5	104,4x75,0x12x12	119,3x89,3x11x11	630	570
2	6.6	8,5	8,5	131,5x84,6x13x13	228,8x98,8x14x14	630	570
3	6.6	9,5	9,5	140,5x84,3x15x15	262,7x167,7x16x16	630	570
4	4.95	9,3	9,3	133,0x79,8x14x14	383,8x173,9x19x19	630	570
5	4.95	10,8	10,8	132,2x79,3x14x14	422,5x172,6x19x19	630	570
6	4.95	11,3	11,3	133,8x80,3x14x14	444,4x174,5x20x20	630	570
7	4.95	11,2	11,2	143,5x80,7x14x14	475,1x175,1x21x21	630	570
8	4.95	11,5	11,5	149,6x84,2x16x16	505,6x175,6x22x22	630	570
9	4.95	12,4	12,4	156,4x82,8x17x17	533,3x173,5x22x22	630	570
10	4.95	12,5	12,5	169,9x85,0x17x17	566,9x176,9x23x23	630	570
11	4.5	14,0	14,0	158,6x79,3x16x16	649,1x189,5x23x23	630	570
12	4.5	13,9	13,9	157,2x78,6x16x16	688,5x188,9x23x23	630	570

The final structural weight for this iteration was calculated to 442mT. The weight with brackets and additional welding weight was 483 mT.

Appendix B: Stresses in transverse direction

A stresses plot in the transverse direction in this section is taken from Jens (2012) [15] used in the present study for analysing buckling and yielding. The local lateral pressure due to setback loads in the most critical load case, quart sea, is presented in this plot.
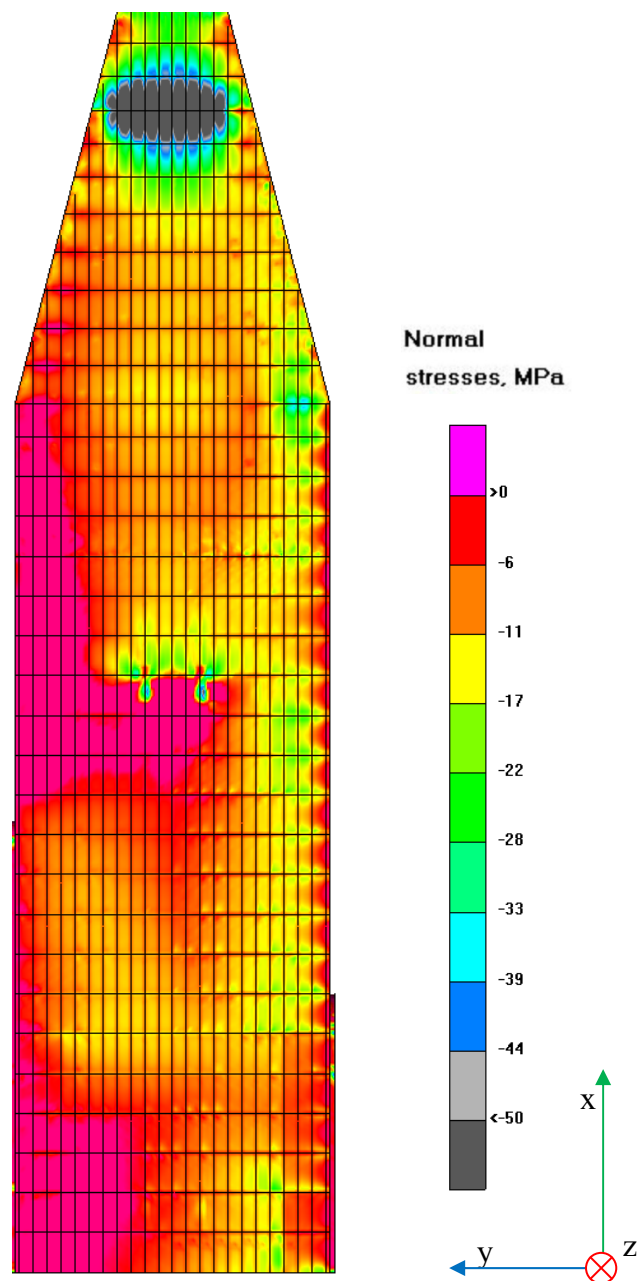
Figure B.1   Stresses in the transverse direction, starboard from [15].

Appendix C: Cost for stressed skin derrick

The cost calculation here in Appendix C according to Farkas [32] determines the important parameters for cost determination. The cost of materials F_{mat} means the steel acquisition cost. For a stiffened panel, the cost was directly derived from the structural weight using the following equation (C.1).

$$F_{mat} = 2\gamma\, L_i\, B_i \cdot \left[C_1\delta + C_2\left(h_w t_w + b_f t_f\right)X + C_3\left(h_w t_w + b_f t_f\right)Y \right] \qquad \text{(C.1)}$$

where,

F_{mat}	=	total cost of materials	NOK
γ	=	steel specific weight	kg/m^3
L	=	stiffened panel length	m
B	=	stiffened panel width	m
δ	=	plate thickness	m
h_w	=	web height, stiffener/stringer	m
t_w	=	web thickness, stiffener/stringer	m
b_f	=	flange width, stiffener/stringer	M
t_f	=	flange thickness, stiffener/stringer	m
X	=	number of longitudinal stiffeners	-
Y	=	number of transversal frames	-
C_1	=	cost of a plate with δ-thickness	NOK/kg
C_2	=	cost of longitudinal stiffeners	NOK/kg
C_3	=	cost of transversal frames	NOK/kg

The total material costs for a stressed skin derrick were estimated to 7.82 MNOK and the total cost estimation is presented in Table C.1.

Table C.1   Material cost calculation for a stressed skin derrick.

Seg.	L_{head}	L_{beam}	B	C_1	C_2	C_3	Number of stiffener head	Number of stiffener beam	Cost head [NOK]	Cost beam [NOK]
1	15.85	14.0	6.6	2.63	3.38	3.0	7	6	124 642	100 337
2	15.85	14.0	6.6	2.63	3.38	3.0	11	9	205 289	156 644
3	15.85	14.0	4.95	2.63	3.38	3.0	15	12	347 965	258 178
4	15.85	14.0	4.95	2.63	3.38	3.0	20	17	245 101	192 346
5	15.85	14.0	4.95	2.63	3.38	3.0	20	17	301 899	238 116
6	15.85	14.0	4.95	2.63	3.38	3.0	20	17	328 421	256 281
7	15.85	14.0	4.95	2.63	3.38	3.0	20	17	321 107	251 797
8	15.85	14.0	4.95	2.63	3.38	3.0	20	17	370 532	289 416
9	15.85	14.0	4.95	2.63	3.38	3.0	20	17	402 125	308 335
10	15.85	14.0	4.95	2.63	3.38	3.0	20	17	447 665	345 918
11	15.85	14.0	4.5	2.63	3.38	3.0	25	22	420 911	337 357
12	15.85	14.0	4.5	2.63	3.38	3.0	25	22	461 971	369 733
								Sum	3977 629	3104 458
								F_{mat}		**7.82 MNOK**

The cost of consumables means the cost of welding, except for labour costs and is composed of the cost of energy, gas, and electrodes provision for equipment depreciation. The cost of consumables for a stiffened panel was calculated from equation (C.2).

$$F_{cons} = L \cdot B \cdot \left(2 - \alpha_X \cdot C_X + 2 - \alpha_Y \cdot C_Y\right) \qquad \text{(C.2)}$$

where,

F_{cons}	=	total cost of consumables	MNOK
L	=	stiffened panel length	m
B	=	stiffened panel width	m
α_X	=	binary coefficient for stiffeners	-
α_Y	=	binary coefficient for frames	-
C_X	=	consumables cost for long. stiffeners welding	NOK/m
C_Y	=	consumables cost for trans. frames welding	NOK/m

The cost of consumables of the stressed skin derrick was calculated to 0.170 MNOK and the result is utilized in Table C.2.

Table C.2   Consumables cost calculation for stressed skin derrick.

Seg.	L	B	α_X	α_Y	C_X	C_Y	Cost head [NOK]	Cost beam [NOK]
1	15.85	14.00	1.00	0.00	15.00	15.00	9415	8316
2	15.85	14.00	1.00	0.00	15.00	15.00	9415	8316
3	15.85	14.00	1.00	0.00	15.00	15.00	9415	8316
4	15.85	14.00	1.00	0.00	15.00	15.00	7061	6237
5	15.85	14.00	1.00	0.00	15.00	15.00	7061	6237
6	15.85	14.00	1.00	0.00	15.00	15.00	7061	6237
7	15.85	14.00	1.00	0.00	15.00	15.00	7061	6237
8	15.85	14.00	1.00	0.00	15.00	15.00	7061	6237
9	15.85	14.00	1.00	0.00	15.00	15.00	7061	6237
10	15.85	14.00	1.00	0.00	15.00	15.00	7061	6237
11	15.85	14.00	1.00	0.00	15.00	15.00	6419	5670
12	15.85	14.00	1.00	0.00	15.00	15.00	6419	5670
						Sum	9415	8316
						F_{cons}	**0.170MNOK**	

The labour costs are related to the workload for welding and welding surface preparation. For a stiffened panel, labour was estimated according to Equation (C.3).

$$F_{lab} = C \cdot Wload \tag{C.3}$$

where,

F_{LAB}	=	total cost of operators	NOK
C	=	cost of operation	NOK/hour
$Wload$	=	workload required for the fabrication of the stiffened panel	Man-hour

The amount of workload was calculated with equation (C.4).

$$WLoad = L \cdot B \cdot \left[P_4 + P_5 + P_6 + P_7 + P_{10} \right] \tag{C.4}$$

where,

P_4	=	workload for welding of long. stiffeners web on the plate	Man-hour/m
P_5	=	workload for welding of trans. frames web on the plate	Man-hour/m
P_6	=	workload required for welding and preparation of one intersection between long. stiffeners and transversal frames	Man-hour/ inters.
P_7	=	workload required for fixing the brackets at one intersection between long. stiffeners and transversal frames	Man-hour/inters.
P_{10}	=	workload required for the preparation of plate	Man-hour/m²

The costs for operators of the stressed skin derrick were calculated to 26.12 MNOK and for detailed results, see Table C.3

Table C.3   Labour cost calculation for a stressed skin derrick.

Segm.	C	P4	P5	P6	P7	P10
1	75	0.5	1.2	0.25	1.3	0.1
2	75	0.5	1.2	0.25	1.3	0.1
3	75	0.5	1.2	0.25	1.3	0.1
4	75	0.5	1.2	0.25	1.3	0.1
5	75	0.5	1.2	0.25	1.3	0.1
6	75	0.5	1.2	0.25	1.3	0.1
7	75	0.5	1.2	0.25	1.3	0.1
8	75	0.5	1.2	0.25	1.3	0.1
9	75	0.5	1.2	0.25	1.3	0.1
10	75	0.5	1.2	0.25	1.3	0.1
11	75	0.5	1.2	0.25	1.3	0.1
12	75	0.5	1.2	0.25	1.3	0.1